



Journal of Ata-Chem Ata-Kimya Dergisi

Offical Journal of Atatürk University Faculty of Science

Volume/Cilt 5. Issue/Sayı 1. May/Mayıs 2025



Journal of Ata-Chem

EDITOR / EDITÖR

Elif ŞENKUYTU 🕒

Department of Chemistry, Atatürk University, Erzurum, Turkey Atatürk Üniversitesi-Kimya Bölümü, Erzurum, Türkiye

ASSOCIATE EDITOR / YARDIMCI EDİTÖR

Ömer İrfan KÜFREVİOĞLU

Department of Chemistry, Atatürk University, Erzurum, Turkey Atatürk Üniversitesi-Kimya Bölümü, Erzurum, Türkiye

TECHNICAL EDITOR / TEKNIK EDITÖR

Esra TANRIVERDI EÇIK

Department of Chemistry, Atatürk University, Erzurum, Turkey Atatürk Üniversitesi-Kimya Bölümü, Erzurum, Türkiye

LANGUAGE EDITOR / DİL EDİTÖRÜ

Süreyya Oğuz TÜMAY

Department of Chemistry, Atatürk University, Erzurum, Turkey Atatürk Üniversitesi-Kimya Bölümü, Erzurum, Türkiye

STATISTICS EDITOR / İSTATİSTİK EDİTÖRÜ

Melike SEVİM

Department of Chemistry, Atatürk University, Erzurum, Turkey Atatürk Üniversitesi-Kimya Bölümü, Erzurum, Türkiye

EDITORIAL and ADVISORY BOARD / YAYIN ve DANIŞMA KURULU

Gönül YENİLMEZ ÇİFTÇİ 🕒

Department of Chemistry, Gebze Technical University Kocaeli, Türkiye Gebze Teknik Üniversitesi, Kimya Bölümü, Kocaeli, Türkiye

Derya DAVARCI

Department of Chemistry, Gebze Technical University Kocaeli, Türkiye Gebze Teknik Üniversitesi, Kimya Bölümü, Kocaeli, Türkiye

Tuba YILDIRIM®

Department of Biology, Amasya University, Amasya, Türkiye Amasya Üniversitesi, Biyoloji Bölümü, Amasya, Türkiye

Erdinç DOĞANCI

Department of Chemistry and Chemical Processing Technologies, Kocaeli University, Kocaeli, Türkiye Kocaeli Üniversitesi, Kimya ve Kimyasal İşleme Teknolojileri Bölümü, Kocaeli, Türkiye

Kenan KORAN D

Department of Food Technology,Fırat University, D Elazığ, Türkiye Fırat Üniversitesi, Gıda Teknolojisi Bölümü, Elazığ, Türkiye

Mehmet PİŞKİN 匝

Food Processing, Çanakkale Onsekiz Mart University, Çanakkale, Türkiye Çanakkale Onsekiz Mart Üniversitesi, Gıda İşleme, Çanakkale, Türkiye

Semra KARACA

Department of Chemistry, Atatürk University, Erzurum, Turkey Atatürk Üniversitesi-Kimya Bölümü, Erzurum, Türkiye

Nurhan KISHALI

Department of Chemistry, Atatürk University, Erzurum, Turkey Atatürk Üniversitesi-Kimya Bölümü, Erzurum, Türkiye

Deryanur KILIÇ®

Department of Chemistry, Atatürk University, Erzurum, Turkey Atatürk Üniversitesi-Kimya Bölümü, Erzurum, Türkiye

Tuba ÖZNÜLÜER 🕒

Department of Chemistry, Atatürk University, Erzurum, Turkey Atatürk Üniversitesi-Kimya Bölümü, Erzurum, Türkiye



Journal of Ata-Chem

ABOUT

Journal of Ata-Chem is a peer reviewed, open access, online-only journal published by the published by Atatürk University.

Journal of Ata-Chem is published biannual in Turkish and English in May, and November.

Abstracting and Indexing

Journal of Ata-Chem is covered in the following abstracting and indexing databases;

- DOAJ
- Gale Cengage

Journal of Ata-Chem aims to publish studies of the highest scientific and clinical value in all areas of chemistry.

Journal of Ata-Chem publishes research articles, reviews, letters to the editors, and short articles that will contribute to the literature on chemistry. The main purpose of the journal is to disseminate the scientific knowledge produced in the field of analytical chemistry, biochemistry, biotechnology, inorganic chemistry, organic chemistry, physical chemistry, chemical engineering, food chemistry, materials science, polymer chemistry, environmental chemistry, energy technologies, pharmaceutical chemistry, plant science, medicinal chemistry, forensic chemistry, theoretical chemistry, nanotechnology, agricultural chemistry and geochemistry to a wide platform. In doing so, the journal aims to bring together researchers, educational practitioners and policy makers at a common intersection.

The target audience of the journal includes academicians, clinical researchers, medical/health professionals, students, and related professional and academic bodies and institutions.

All published content is available online, free of charge at https://dergipark.org.tr/en/pub/atakim.

HAKKINDA

Ata-Kimya Dergisi, hakemli, acık erisimli ve yalnızca çevrimici olarak Atatürk Üniversitesi tarafından yayınlanan bir dergidir.

Ata-Kimya Dergisi, Mayıs ve Kasım aylarında, İngilizce ve Türkçe olarak yılda iki kez yayınlanan bir dergidir.

Özetleme ve İndeksleme

Ata-Kimya Dergisi aşağıdaki özetleme ve indeksleme veri tabanlarında yer almaktadır:

- DOAJ
- Gale Cengage

Ata-Kimya Dergisi, kimyanın tüm alanlarında bilimsel ve klinik değeri en yüksek çalışmaları yayınlamayı amaçlamaktadır.

Ata-Kimya Dergisi, kimya ilgili literatüre katkı sunacak, özellikle araştırma makaleleri, derlemeler, editöre mektuplar ve kısa makaleler yayınlamaktadır. Derginin temel amacı, analitik kimya, biyoteknoloji, anorganik kimya, organik kimya, fizikokimya, kimya mühendisliği, gıda kimyası, malzeme bilimi, polimer kimyası, çevre kimyası, enerji teknolojileri, ilaç kimyası, bitki bilimi, tıbbi kimya, adli kimya, teorik kimya, nanoteknoloji, zirai kimya ve jeokimya alanında üretilen bilimsel bilgiyi geniş bir platforma yaymaktır. Dergi bunu yaparken araştırmacıları, eğitim uygulayıcılarını ve politika yapıcılarını ortak bir kesişim noktasında buluşturmayı hedeflemektedir.

Derginin hedef kitlesi akademisyenler, klinik araştırmacılar, tıp/sağlık profesyonelleri, öğrenciler ve ilgili mesleki ve akademik kurum ve kuruluşlardan oluşmaktadır.

Tüm yayımlanan içerikler https://dergipark.org.tr/tr/pub/atakim adresinden çevrimiçi olarak üçretsiz olarak erişilebilir.



Contact (Editor in Chief) / İletişim (Baş Editör)

Elif ŞENKUYTU

Atatürk University, Department of Chemistry, Erzurum, Turkey Atatürk Üniversitesi, Kimya Bölümü, Erzurum, Türkiye

<u>elif.senkuytu@atauni.edu.tr</u>

⊠ jof.atachem@atauni.edu.tr

• https://dergipark.org.tr/tr/pub/atakim

2 +90 442 231 4114

Contact (Publisher) / İletişim (Yayıncı)

Atatürk University

Atatürk University, Erzurum, Turkey Atatürk Üniversitesi Rektörlüğü 25240 Erzurum, Türkiye

ataunijournals@atauni.edu.tr

https://bilimseldergiler.atauni.edu.tr

***** +90 442 231 15 16

Journal of Ata-Chem

CONTENTS / İÇİNDEKİLER

Research Articles/Araştırma Makaleleri

- Yeni Fosfino Metalosen Ditiyofosfonato Nikel Kompleksinin Sentezi ve Yapısının Aydınlatılması
 Synthesis and Structural Investigation of a New Phosphino Metallocene Dithiophosphonato Nickel Complex
 Elif BULAT, Ezgi GÜLEN, Ertuğrul Gazi SAĞLAM
- 10 Kinetik Analiz Yöntemi Kullanılarak Sulu Asidik Fazda Sülfit İyonlu Krizoidin Y Boyasının Bozunması

 Degradation of Chrysoidine Y Dye with Sulphite Ion in Aqueous Acidic Phase using Kinetic Method of Analysis

 Patricia Ese UMORU, Ikechukwu Ugbaga NKOLE
- Zerdeçal ve Zencefil Özleri Karışımının Çevre Dostu Doğal Boyalar Olarak Kullanımı The use of Turmeric and Ginger Extracts Mixture as Eco-Friendly Natural Dyes
 K. Ceren TOMBUL APARDIM, Adem ÖNAL, Mehmet Emin ÇAKMAK, Sedanur GÖKÇE
- SARS-COV-2 Papain Benzeri Proteaz (PLpro) İçin Yeni İnhibitörlerin Sanal Tarama ve Moleküler Yerleştirme Çalışması
 The Virtual Screening and Molecular Docking Study of New Inhibitors for SARS-COV-2 Papain-Like Protease (PLpro)
 Alev ARSLANTÜRK BİNGUL, Necmettin PİRİNCCİOGLU





Yeni Fosfino Metalosen Ditiyofosfonato Nikel Kompleksinin Sentezi ve Yapısının Aydınlatılması

Synthesis and Structural Investigation of a New Phosphino Metallocene Dithiophosphonato Nickel Complex

ÖZ

Metalosen içerikli bilinen bir ferrosenilditiyofosfonato Ni(II) kompleksinin [Ni(FcL)₂], (FcL= O-1-fenil-1-propil (ferrosenil)ditiyofosfonat), bis(difenilfosfino)metan (DPPM) ve Na[B(Ph)₄] ile reaksiyonundan yeni bis-(difenilfosfino)metan[O-1-fenil-1-propil(ferrosenil)ditiyofosfonato]Ni(II)tetrafenilborat ([Ni(FcL)(DPPM)]⁺[BPh₄]⁻), iyonik kompleksi sentezlendi. Kompleksin yapısı element analizi, titreşim spektroskopisi (FT-IR ve Raman), MS (MALDI-TOF) ve ³¹P- NMR yöntemleriyle karakterize edildi. ³¹P-NMR analizi, spektrumdaki fosfor atomunun alan integrallerinin molekülde üç fosfor atomu olduğunu doğrulamaktadır.

Anahtar Kelimeler: Ferrosenil Ditiyofosfonik asitler, Fosfonoditiyoato Ni(II) kompleksleri, Tetrafenilborat, Fosfin Ligandları

ABSTRACT

A new bis-(diphenylphosphino) methan [O-1-phenyl-1-propyl (ferrocenyl) dithiophosphonate] Ni(II) tetraphenylborat ([Ni(FcL)(DPPM)]+[BPh4]-; FcL= O-1-phenyl-1-propyl(ferrocenyl)dithiophosphonates, DPPM= bis(diphenylphosphino)methane), ionic complex was synthesized from the reaction of ferrocenyldithiophosphonato Ni(II) complex containing metallocene [Ni(FcL)₂] which is known with DPPM and Na[B(Ph)₄]. The structure of the synthesized complex was characterized by elemental analysis, vibrational spectroscopy (FT-IR and Raman), MS (MALDI-TOF) and ³¹P-NMR methods. Spectroscopic methods confirm the suggested structure. ³¹P-NMR analysis confirms that the field integrals of the phosphorus atom in the spectrum have three phosphorus atoms in the molecule.

Keywords: Ferrocenyl Dithiophosphonic acids, Phosphonodithioato Ni(II) complexes, Tetraphenylborate, Phosphine ligands

Giriş

Ditiyofosfonat anyonları ve asitleri, DTPOA, Lewis asidi karakteri gösteren ana grup ve geçiş metal iyonlarıyla kompleks oluşturabilen orta sert donör ligandlardır. Bu tür ligandların sentezinde çıkış maddesi olarak genellikle 1,3,2,4 ditiyafosfetan 2,4 disülfürler reaksiyonlarda kullanılır. Bu bileşikler ilk kez Berzelius bileşiğinin (P4S10) bir alifatik reaktifle (siklohegzan) reaksiyon yöntemiyle elde edildi. DTPOA'lerin endüstrideki önemlerinin anlaşılmasıyla^{3,4} ilerleyen yıllarda başlangıç maddesi 1,3,2,4 ditiyafosfetan 2,4 disülfürler için farklı yöntemler geliştirilse de⁵⁻⁹ Berzelius Reaksiyon Yöntemi, araştırmacılar tarafından daha çok tercih edilmiştir. Günümüzde bu bileşikler ticari olarak temin edilebildiği gibi (Lawesson reaktifi, LR gibi; 2,4-bis-(4-metoksifenil)-1,3-ditiya-2,4-difosfetan 2,4- disülfür) ferrosenil awesson reaktifi (2,4-bis-

Elif BULAT ¹
Ezgi GÜLEN ¹
Ertuğrul Gazi SAĞLAM ¹

¹Marmara Üniversitesi, Fen Fakültesi, Kimva Bölümü, İstanbul, Türkive



Geliş Tarihi/Received07.03.2024Kabul Tarihi/Accepted24.06.2024Yayın Tarihi/Publication21.05.2025

Sorumlu Yazar/Corresponding author: *Ertuğrul Gazi SAĞLAM,*

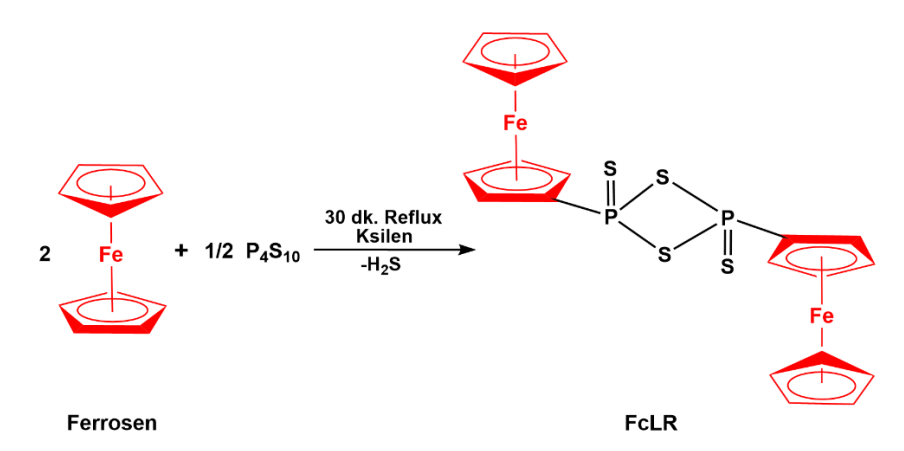
E-mail: saglameq@gmail.com

Cite this article: Bulat E, Gülen E, Sağlam EG. Synthesis and Structural Investigation of a New Phosphino Metallocene Dithiophosphonato Nickel Complex. J Ata-Chem. 2025;5(1): 1-9.



Content of this journal is licensed under a Creative Commons Attribution-Noncommercial 4.0 International License.

(ferrosenil)-1,3-ditiya-2,4-difosfetan 2,4-disülfür, FcLR) gibi laboratuvar ortamında sentezlenebilmektedir (Şekil 1). 10,11



Şekil 1. FcLR sentez reaksiyonu.

DTPOA'ler 1,3,2,4 ditiyafosfetan 2,4 disülfürlerin bir alkolle nükleofilik reaksiyonundan sentezlenir.¹⁰ DTPOA'lerin sentezinde çıkış maddesi olarak LR sıklıkla kullanılır.

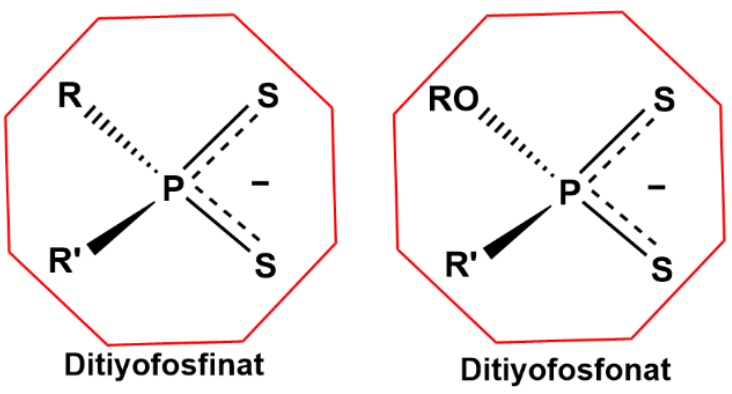
FcLR; LR olduğu gibi, alkollerle reaksiyonundan metalosen içerikli ferrosenil ditiyofosfonik asitlerini (Fc-DTPOA) verirler. 11-13

Fc-DTPOA'lerin yapısındaki sülfür atomlarından dolayı şelat türünde ligandlardır. Bu ligandların metallerle reaksiyonundan, ferrosenil içerikli, farklı çift metal merkezli

(heterobinükleer) kompleksler sentezlenir. ^{10,14} Bu komplekslerden en iyi bilinen kare düzlem yapıdaki tek metal merkezli Ni(II) kompleksleridir, ([Ni(Fc-DTPOA)₂]). ¹⁵ Halkalı ve düzgün dört yüzlü yapıdaki heterobinükleer Cd(II) veya Hg(II) kompleksleri ise farklı çift metal merkezli kompleksleridir. ¹⁶

Ni-DTPOA komplekslerine benzer şekilde [Ni(Fc-DTPOA)₂] kompleksleri de, piridin gibi Lewis bazlarıyla altı koordinasyonlu DTPOA komplekslerini verir (Şekil 2).¹⁷

Şekil 2. Altı koordinasyonlu [Ni(Fc-DTPOA)₂(Py)₂] sentez reasiyonu.



R, R' = H ve aynı/çeşitli türdeki alifatik/aromatik bağlı grupları

Şekil 3. DTPA ve DTPOA Ligandları.

Dört ve altılı koordinasyonlu DTPOA kompleksleri nötr olabildiği gibi, iyonik yapılıda olabilir. 16

DTPOA ligandlarında olduğu gibi ditiyofosfinat türündeki ligandlarda (DTPA) şelat özelliği taşır (Şekil 3). Bu liganlarda DTPOA'ler gibi benzer yapılarda koordinasyon bileşikleri yapar.¹⁸

DTPA anyonları ayrıca fosfin içerikli nötr yapıda¹⁹ veya arilboratlarla fosfin içerikli tuz formunda²⁰ kompleksleri vardır. Ancak iyonik yapılı fosfin grubu içeren ferrosenil ditiyofosfonik asit komplekslerine literatürde rastlanmamıştır.

Bu çalışmada; köprülü bir fosfin ligandının, bilinen dört koordinasyonlu Ni(II) ditiyofosfonato kompleksiyle (trans-[O-1-fenil-1-propil (ferrosenil) ditiyofosfonato] nikel(II); [Ni(FcL)₂]) reaksiyonundan¹⁵ iyonik yeni bir kompleksi sentezlenmiştir (bis-(difenilfosfino)metan [O-1-fenil-1-propil (ferrosenil) ditiyofosfonato] Ni(II) tetrafenilborat, ([Ni(FcL)(DPPM)]⁺[BPh₄]⁻) sentezlendi (Şekil 4). Kompleksin anyon kısmı [BPh₄]⁻ ile oluşturuldu. Kompleksin yapısı; element analizi, FT-IR spektroskopisi, Raman, ³¹P- NMR yöntemleriyle aydınlatıldı.

$$H_3C$$

$$P$$

$$S$$

$$S$$

$$O$$

$$CH_3$$

$$1. + (C_6H_5)_2PCH_2P(C_6H_5)_2$$

$$2. + Na(BPh_4)$$

$$-FcL$$

$$P$$

$$Ni(FcL)_2$$

$$[Ni(FcL)_2]$$

$$[Ni(FcL)(DPPM)]^*[BPh_4]^-$$

Şekil 4. Yeni [Ni(FcL)(DPPM)]⁺[BPh₄]⁻ kompleksinin sentezi.

YÖNTEMLER

Kimyasallar ve Cihazlar

Ferrocene, 1-fenil-1-propanol, metanol, kloroform, bis(difenilfosfino)metan ve Na[B(Ph)₄] Merck firmasından

temin edildi. [Ni(FcL)₂] kompleksi¹⁶ literatürdeki yönteme göre sentezlendi. [Ni(FcL)(DPPM)]+[BPh₄]- kompleksi için literatürdeki yöntem uygulanarak sentezlendi.

Bileşiklerin erime noktası (EN), Electrothermal 9200 cihazında yapıldı. Element analizi, LECO 932 CHNS-O Elementel Analiz cihazında yapıldı. Kütle ölçümleri MALDI-

MS (Bruker marka LT MALDI-TOF MS) tarafından sağlanan bir cihaz gerçekleştirildi. IR spektrumu, Perkin Elmer marka Spectrum Two FT-IR model ATR modüllü cihazında (4000-200 cm⁻¹) ve Raman spektrumu Renishaw İnvia Raman Mikroskobunda alındı. ³¹P-NMR spektrumu Varian Mercury (Agilent) 400 MHz marka cihazında alındı.

Bis-(difenilfosfino)metan[O-1-fenil-1propil(ferrosenil)ditiyofosfonato]Ni(II)tetrafenilborat Kompleksinin Sentez Yöntemi

100 mL'lik bir beher içerisinde, 0.5 g (1 mmol) trans-[O-1-fenil-1-propil (ferrosenil) ditiyofosfonato Ni(II)] kompleksinin etil alkol çözeltisine (~15 mL), bis(difenilfosfino)metanın stokiyometrik miktardaki (1 mmol, 0.22 g) metil alkoldeki çözeltisi (~10 mL) damla damla ilave edildi. Oluşan karışım 5 dk hafif ısıtıldı (~40 °C) ve süzüldü.

Süzüntüye katı Na[BPh4] (1 mmol, 0,20 g) ilave edildi, oda sıcaklığında soğutuldu ve tekrar süzüldü. Süzülen katı, soğuk metil alkolde yıkandı ve vakum desikatöründe kurutuldu. Komplekse ait analitik veriler aşağıdadır:

TARTIŞMA

Titreşim Spektroskopisinde, fosfor ve kükürt bağlarına ait simetrik ve asimetrik fosfor-kükürt gerilme-titreşim bandlarının ($\nu(PS)$) spektrumda 538-600 cm⁻¹ arasında çıkmaktadır. Bu piklerin spektrumda görülmesi Organoditiyofosfor bileşiğinin oluşumunu gösterir. Kompleksin PS simetrik ve asimetrik gerilme titreşim bandlarına ($\nu(PS)_{sym}$ ve $\nu(PS)_{asym}$) ait değerler FT-IR spektrumunda sırasıyla; 538 cm⁻¹ ve 600 cm⁻¹ arasında görülürken, Raman

spektrumunda bu sinyaller sırasıyla; 536 cm⁻¹ ve 613 cm⁻¹ aralığında görülmektedir.

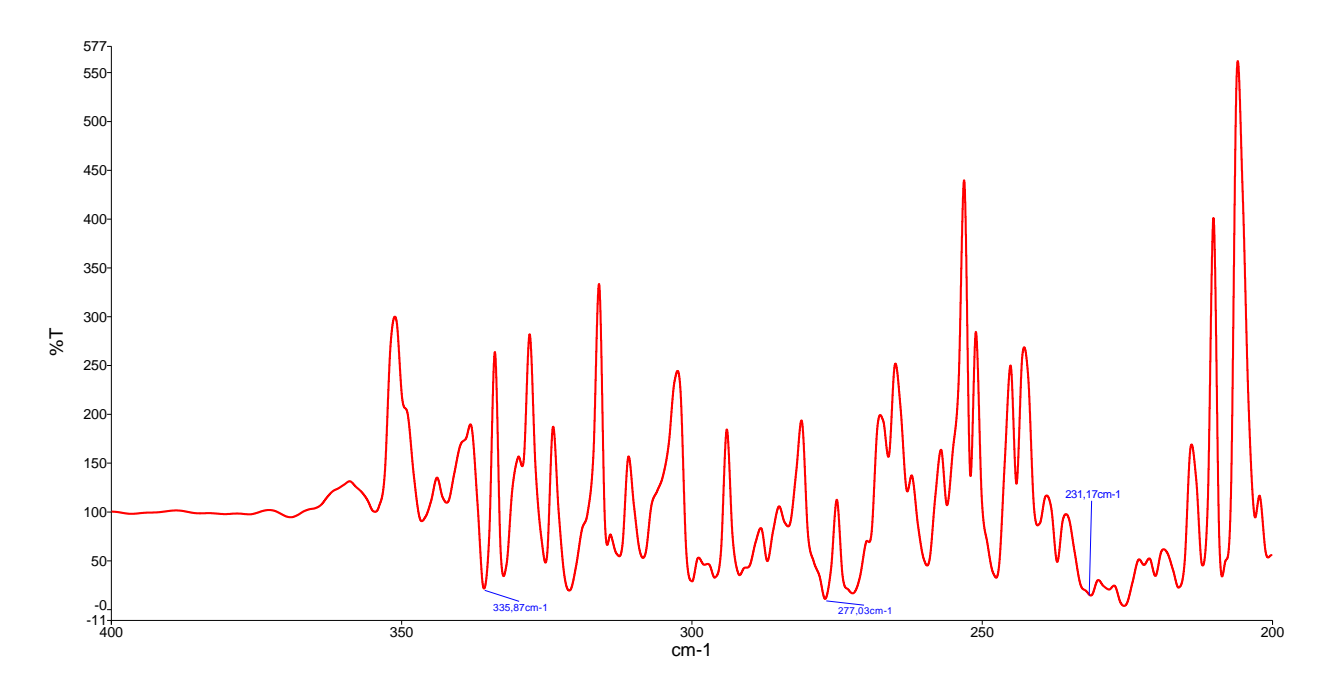
Ayrıca kompleksin FT-IR spektrumunda, simetrik $\nu(Ni-S)_{sym}$ ve asimetrik $\nu(Ni-S)_{asym}$ metal-sülfür gerilme titreşim bandları spektrumun parmak izi bölgesinde 277 cm⁻¹-335 cm⁻¹ aralığında çıkmıştır. Raman spektrumunda ise bu pikler 289 cm⁻¹-330 cm⁻¹ aralığında çıkmıştır (Şekil 5-7). Yine parmak izi bölgesinde nikel-fosfor gerilme titreşim bandları $\nu(Ni-P)$, 230 cm⁻¹-220 cm⁻¹ arasında, beklenildiği gibidir.²¹ Kompleksin IR spektrumunun bu bölgesinde görülen pikler; ayrıca Raman spektrumuyla da doğrulanmaktadır. IR ve Raman spektrumlarındaki değerler benzer çalışmalardaki değerlerle uyum içerisindedir.^{15,18,20}

[Ni(FcL)(DPPM)]⁺[BPh₄] kompleksinin ³¹P-NMR spektrumundaki üç pik (δ = 102.99 ppm, δ = 102.81 ppm ve δ = -33.03 ppm) kimyasal çevresi farklı 3 fosfor atomu olduğunu gösterir. δ = 102.99 ppm ve 102.81 ppm civarında görülen pikler fosfino metandaki metin fosforlarına (-P-CH₂-P-); δ = -33.03 ppm'de çıkan tek pik ise ferrosenil ditiyofosfonato ligandındaki fosfor atomuna (Fc-P-S(S)-) aittir.

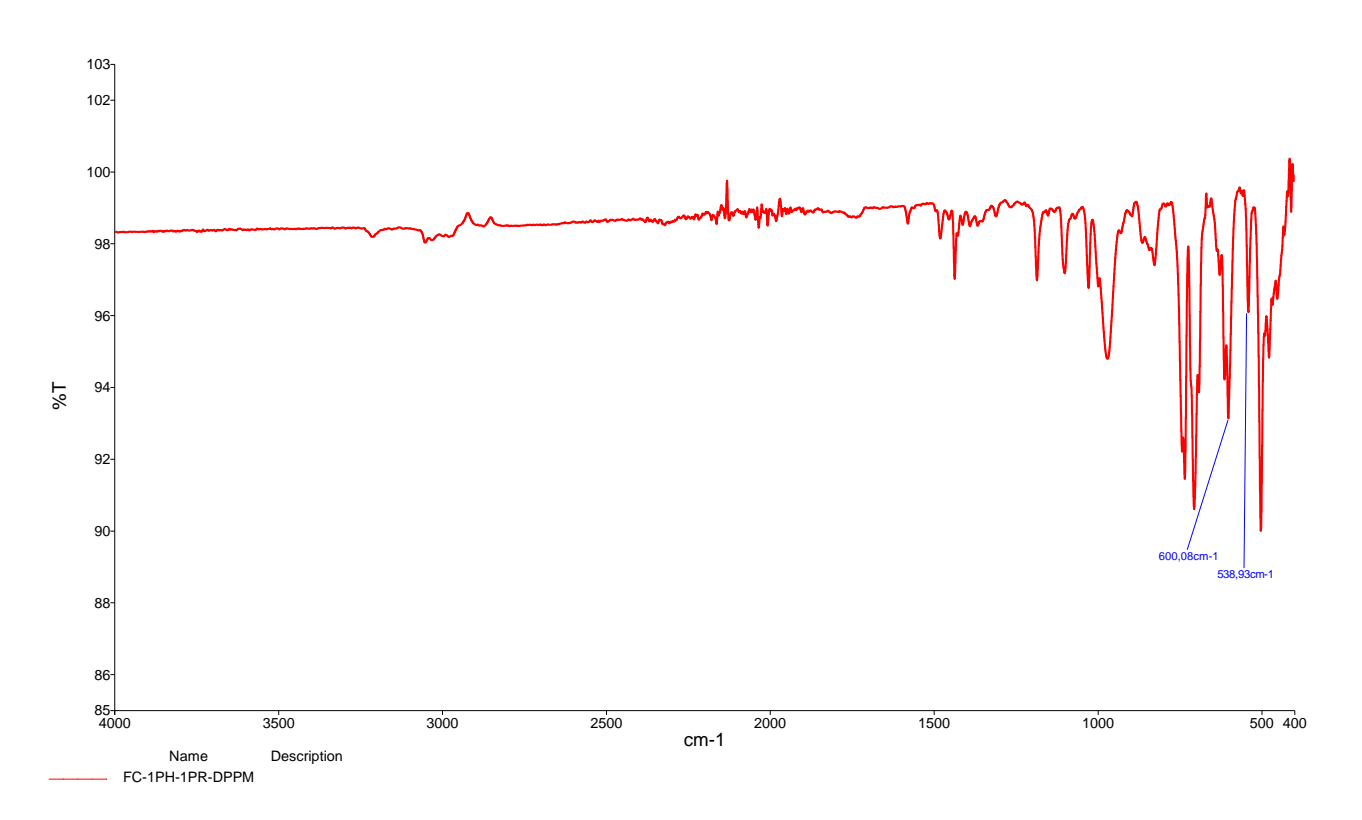
Ligandın ³¹P-NMR spektrumunda δ = -33.03 ppm de görülen tekli pik, fosfino fosforlarıyla (-**P**-CH₂-**P**-) üç bağ öteden eşleşmemiş fosfor atomuna aittir. Anyonik ditiyofosfonato yapılarında bu duruma benzer yapılarda rastlanılmaktadır. ^{20,22} Diğer yandan spektrumda fosfino grubunun fosforları birbirine bitişiktir. Bu fosforlardan biri, diğer fosfino grubundaki fosfor atomu tarafından iki bağ öteden etkileşerek (${}^2J_{P-P}$ = 35.12 Hz) ikili pik olarak çıkmıştır (δ = 102.88 ppm ve δ = 102.73 ppm). İlginçtir ki fosfino fosforları (-**P**-CH₂-**P**), ferrosenil ditiyofosfonato ligandındaki fosforu tarafından etkileşmemiştir. Zaten iki bağ öteden etkileşme sabitinin değeri (${}^2J_{P-P}$ = 35.12 Hz), üç bağ öteden etkileşme sabitinin değerinden (19,20 , (${}^3J_{P-P}$ = 7.3-6.8 Hz) yüksektir. Spektrumda fosfor atomuna ait alan integralleri, molekülde üç fosfor atomunun olduğunu doğrulamaktadır.

Tablo 1. [Ni(FcL)(DPPM)]⁺[BPh₄]⁻ kompleksine ait FT-IR ve Raman verileri.

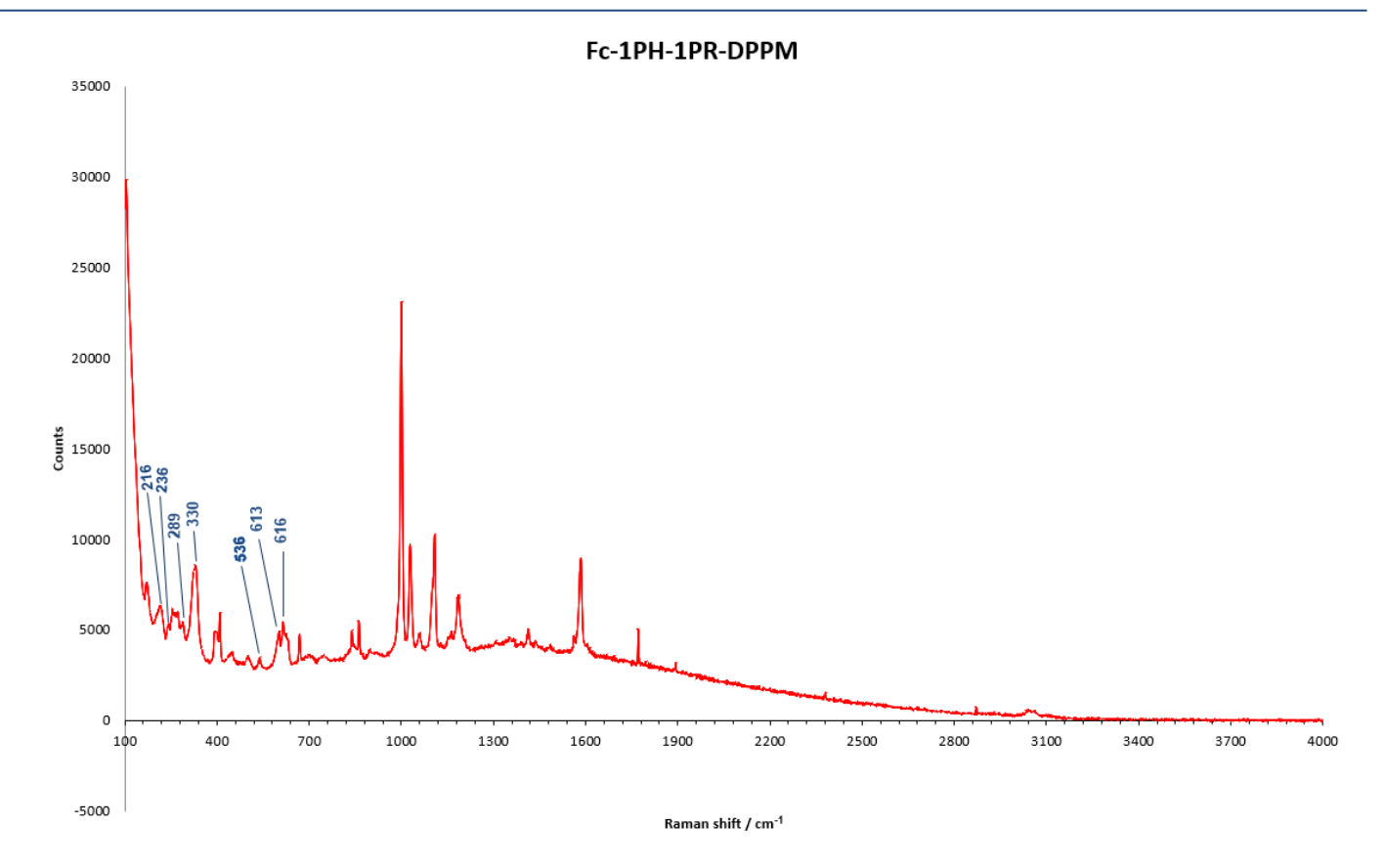
[Ni(FcL)(DPPM)] ⁺ [BPh ₄] ⁻	v(PS) _{sym}		ν(PS) _{asym}		ν(Ni-S) _{sym}		ν(Ni-S) _{asym}		v(Ni-P)	
	IR R		IR	R	IR	R	IR	R	IR	R
cm ⁻¹	538	536	600	613	277	289	335	330	230	236



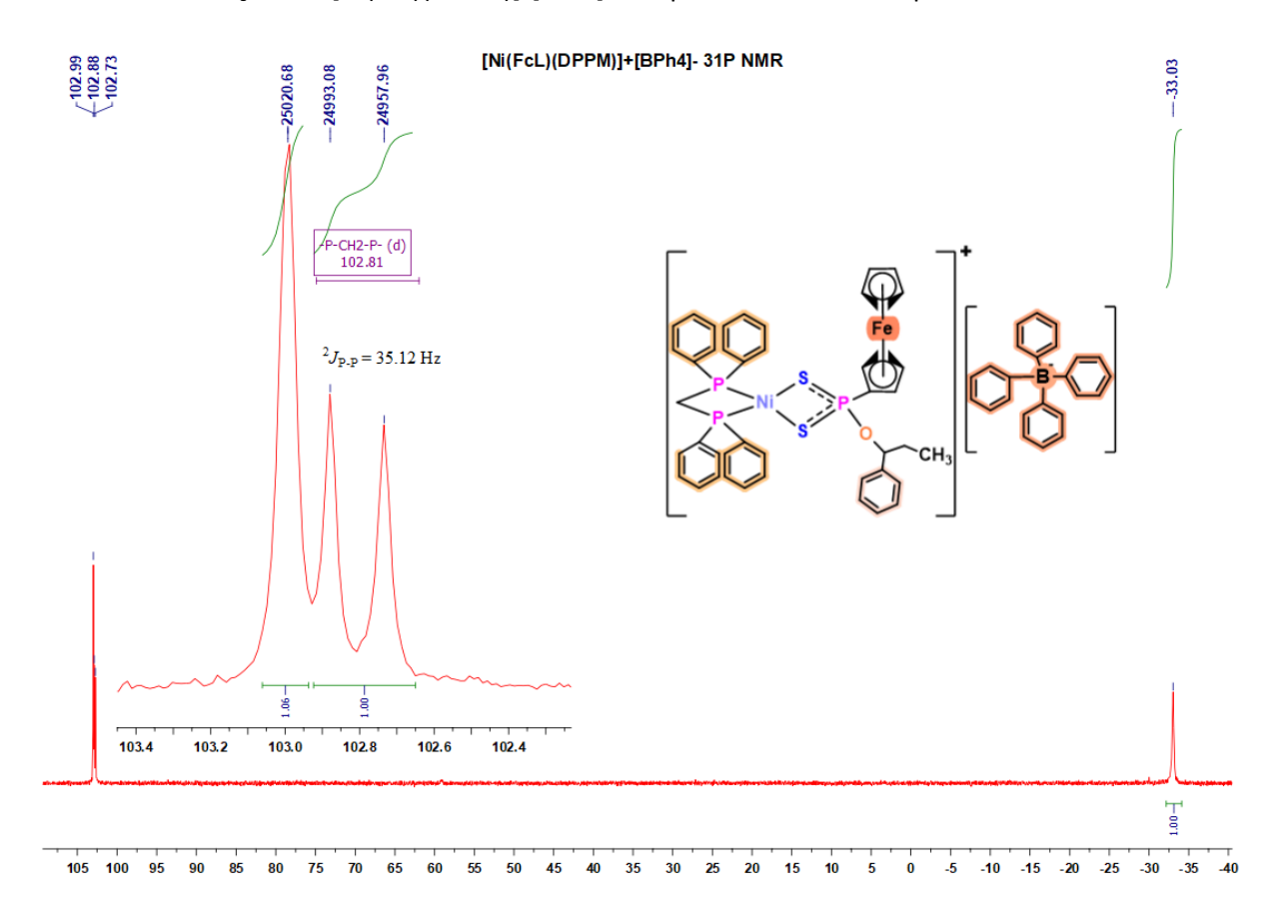
Şekil 5. [Ni(FcL)(DPPM)]⁺[BPh₄]⁻ kompleksine ait FT-IR spektrumu (400-200 cm⁻¹).



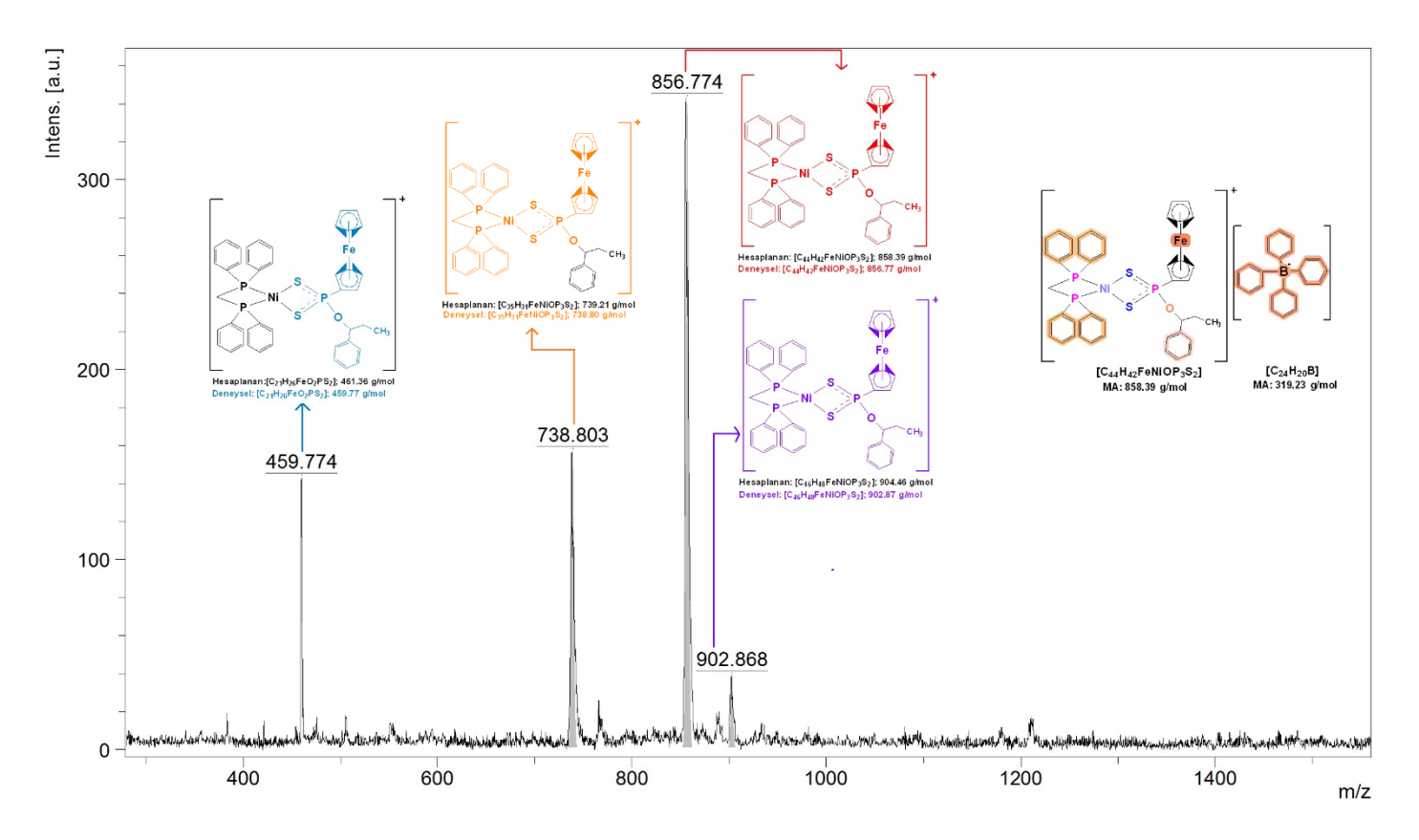
Şekil 6. [Ni(FcL)(DPPM)]⁺[BPh₄]⁻ kompleksine ait FT-IR spektrumu (4000-400 cm⁻¹).



Şekil 7. [Ni(FcL)(DPPM)]⁺[BPh₄]⁻ kompleksine ait Raman spektrumu.



Şekil 8. Bileşiğe ait ³¹P NMR spektrumu.



Şekil 9. Bileşiğe ait kütle spektrumu.

Kompleksin kütle spektrumu Şekil 9'da görülmektedir. Molekül iyon veya bazı fragman pikleri hesaplanan değerin 23, 32, 41 veya 46 birim üzerinde m/z değerlerine sahiptir. Bu, kütle analizi sürecinde kullanılan çözücünün (buffer solution; Na atomu, asetonitril, metanol veya etanolün) moleküle veya molekülden avrılan parcacıklara (fragmentlere) bağlanmasıyla ilgilidir. 12,23-25 Ayrıca molekül pik m/z değerleri bazı atomların izotopları sebebiyle (nikel, demir veya kükürt) beklenen değerden az olsa farklılık durumlara literatürlerde göstermektedir. Benzer rastlanılmaktadır.^{25,26} Molekülün ([M⁺][B(Ph)₄-]) spektrumunda (MALDI-TOF, m/z), molekül katyon kısmı görülmektedir. ([M+], C₄₄H₄₂FeNiOP₃S₂, MALDI-TOF m/z hesaplanan 858.40, deneysel 856, 77). Spektrumda bağıl bolluğu azda olsa [M⁺] parçasına tutunan çözücü piki de (etanol) görülmektedir ([M+C₂H₅OH]⁺, C₄₆H₄₈FeNiO₂P₃S₂, MALDI-TOF m/z hesaplanan 904.46, deneysel 902,87). Ayrıca spektrumda; molekülün katyon kısmından ayrılmış 1-fenil 1 propil- grubu (C₃₅H₃₁FeNiOP₃S₂, MALDI-TOF m/z hesaplanan 739.21, deneysel 738,80) ve O-1-fenil-1-propil (ferrosenil)ditiyofosfonat ligand kısmına tutunmuş etanol çözücü pikide görülmektedir (C21H26FeO2PS2, MALDI-TOF m/z hesaplanan 461.37, deneysel 459,77). Hesaplanan elementel analiz verileriyle deneysel veriler birbirleriyle uyuşmaktadır.

Hakem Değerlendirmesi: Dış bağımsız.

Yazar Katkıları: Elif Bulat, Kavramsallaştırma, Görselleştirme, Hazırlık, Metodoloji, Biçimsel Analiz, Araştırma, Yazma-Orijinal. Ezgi Gülen: Araştırma, Sentezleme, Doğrulama, Yazma, Finansman sağlama. Ertuğrul Gazi Sağlam, Kavramsallaştırma, Doğrulama, Hazırlık, Biçimsel analiz, Araştırma, Kaynaklar, Denetleme, Yazma-Orijinal, Yazma-İnceleme ve Düzenleme, Görselleştirme, Finansman sağlama.

Çıkar Çatışması: Yazarlar, çıkar çatışması olmadığını beyan etmiştir.

Finansal Destek: Yazarlar bu çalışmaya "Üniversite Öğrencileri Araştırma Projeleri Destekleme Programı" kapsamında finansal destekte bulunan, "TÜBİTAK 2209-A" projesine teşekkür ederler.

Peer-review: Externally peer-reviewed.

Author Contributions: Elif Bulat, Conceptualization, Visualization, Preparation, Methodology, Formal Analysis, Investigation, Writing-Original. Ezgi Gülen, Investigation, Synthesizing, Verification, Writing-Original, Funding. Ertuğrul Gazi Sağlam, Conceptualization, Verification, Preparation, Formal analysis, Investigation, Sources, Auditing, Writing-Original, Writing-Review and Editing, Visualization, Funding.

Conflict of Interest: The authors have no conflicts of interest to declare. **Financial Disclosure:** The authors would like to thank the "TUBITAK 2209-A" project, which provided financial support for this study within the scope of the "University Students Research Projects Support Program".

KAYNAKLAR

- Van-Zyl WE. Dithiophosphonates and Related P/S-Type Ligands of Group 11 Metals. Com Inorg Chem. 2010;31:13-45.
- 2. Fay P, Lankelma HP. The Reaction of Cyclohexene with Phosphorus Pentasulfide. *J Am Chem Soc.* 1952;74:4933-4935.
- 3. Contarini S, Tripaldi G, Ponti G, et al. Surface investigation of lubricant—metal interactions by synchrotron photoemission spectroscopy. *App Surf Sci.* 1997;108:359-364.
- Fuller M, Yin Z, Kasrai M, et al. Chemical characterization of tribochemical and thermal films generated from neutral and basic ZDDPs using X-ray absorption spectroscopy. *Tribol Int.* 1997;30:305-315.
- Cava MP, Levinson MI. Thionation Reactions of Lawesson's Reagents. *Tetrahedron*. 1985;41:5061-5087.
- Newallis PE, Chupp JP, Groenweghe LCD. Thionophosphine Sulfides. I. Preparation and Use in the Friedel-Crafts Reaction. *J Org Chem.* 1962;27:3829-3831.
- 7. Sağlam EG, Bulat E, Yılmaz H. The Syntheses and Characterization of New Dithiophosphonates derived from Novel 2,4-Bis(methoxytolyl)-1,3-dithia-2,4-diphosphetane 2,4-disulfides and Their Ni(II) Complexes. *JOTCSA*. 2020;7:789-800.
- 8. Bulat E, Sağlam EG, Zeyrek CT, et al. Ni(II) complexes with 1,3,2,4-dithiadiphosphetane 2,4-disulfide-based ligands: Structural insights, theoretical studies, and anticancer activities. *Appl Organomet Chem.* 2022;36:e6821.
- Bulat E, Sağlam EG, Zeyrek CT, et al. 2,4-Bis(2,4-dimethoxyphenyl)-1,3-dithia-2,4-diphosphetane 2,4-disulfide and its derivatives: Syntheses, structural characterizations, anticancer activities, and theoretical studies on some dithiophosphonato Ni(II) complex. J Mol Struct. 2023;1272:134197.
- 10. Van Zyl WE, Facler JP. A General and Convenient Route to Dithiophosphonate Salt Derivatives. *Phosphorus, Sulfur, Silicon Relat Elem.* 2000;167:117-132.

- 11. Foreman MStJ, Slawin AMZ, Woollins JD. 2, 4-Diferrocenyl-1,3-dithiadiphosphetane 2,4-disulfide; structure and reactions with catechols and [PtCl₂(PR₃)₂] (R= Et or Bun). *J Chem Soc Dalton Trans*. 1996;18:3653-3657.
- 12. Sağlam EG, Akkoç S, Zorlu Y, et al. New phenanthroline nickel(II) organodithio-phosphorus complexes: Syntheses, structural characterizations and in vitro cytotoxic activity studies. *Polyhedron*. 2021;199:1-13.
- 13. Sağlam EG, Erden S, Tutsak Ö, et al. Syntheses, characterization of and studies on the electrochemical behaviour of ferrocenyl dithiophosphonates and 4-methoxyphenyl dithiophosphonates. *Phosphorus, Sulfur, Silicon Relat Elem.* 2017;192:322-329.
- 14. Karakus M, Lonnecke P, Yakhvarov D, et al. Heterobimetallic Nickel(II)Complexes of Ferrocenyldithiophosphonates. Molecular Structures of [{FcP(OR)S $_2$ } $_2$ Ni] [Fc Fe(η^5 -C $_5$ H $_4$)(η^5 -C $_5$ H $_5$), R= Et, Pr $_1$, Bu $_2$, Bu $_3$, Bu $_4$]. Z Anorg Allg Chem. 2004;630:1444-1450.
- 15. Sağlam EG, Akkoç S, Zeyrek CT, et al. New heterobimetallic nickel(II) ferrocenyldithiophosphonato complexes: Syntheses, characterization, antiproliferative activity and X-ray, DFT, molecular docking studies on trans-bis- [O-3-methyl- 1-butyl- (ferrocenyl) dithiophosphonato] nickel(II). Inorg Chim Acta. 2021;514:119991.
- 16. Sağlam EG, Akkoç S, Acar N, et al. New Heterobimetallic Ferrocenyl Dithiophosphonato Cd(II) and Hg(II) Complexes: DNA Interactions, Antimicrobial and Anticancer Activity Studies of the Cd(II) Complexes. *Chemistry Select.* 2021;6:12496-12505.
- 17. Gray IP, Milton HL, Slawin AMZ, et al. Synthesis and structure of $[Fc(RO)PS_2]$ complexes. *Dalton Trans.* 2003;17:3450-3457.
- 18. Sağlam EG., Çelik Ö, Yılmaz H, et al. Synthesis, spectroscopic characterization and X-ray single crystal structures of trans-bis[4-methoxyphenyl (3-methylbutyl) dithiophosphinato] nickel(II) and bis [4-methoxyphenyl (3-methylbutyl) dithiophosphinato] cobalt(II) complexes. *Trans Met Chem.* 2010;35:399-405.

- 19. Esterhuysen C, Kruger GJ, Blewett G, et al. 4-Membered metallodithiophosphinate rings flat or puckered? A comparison of two crystal structures with computational and literature data. *Inorg Chim Acta*. 2006;359:609-616.
- Duffy ST, Nicholson BK, Henderson W. Diisobutyldithiophosphinate complexes of nickel(II), palladium(II) and platinum(II) with ancillary phosphine ligands. J Sulfur Chem. 2011;32:443-450.
- 21. Ferraro JR, Wang JT, Udovich C, et al. Low-frequency infrared spectra of planar and tetrahedral nickel bromide complexes of diphenylalkylphosphines. *Inorg Chem.* 1970;:12:2675-2678.
- 22. Exarchos G, Robinson SD, Steed JW. The synthesis of new bimetallic complex salts by halide/sulfur chelate cross transfer: X-ray crystal structures of the salts [Ni(S₂CNEt₂)(dppe)]₂[HgBr₄], [Pt(S₂CNEt₂) (dppe)]₂ [CdCl₄], [Co(S₂CNEt₂)₂(dppe)]₂ [Cl₃ZnO: (Ph)₂PCH₂CH₂P(Ph)₂: OZnCl₃] and [Pd(S₂CNnBu₂)(bipy)]₂[CdCl₄]. *Polyhedron*. 2001;20:2951-2963.
- 23. Karakus M, Yılmaz H. Synthesis and Characterization of Ni(II), Zn(II), and Cd(II) Complexes with Dithiophosphonate Derivatives. *Russ J Coord Chem.* 2006;32:437-443.
- 24. Heinz S, Keck H, Kuchen W. Mass spectrometric studies of dithiophosphinato metal complexes. *Org Mass Spectrom.* 1984;19:82-86.
- 25. Sağlam EG, Ebinç A, Zeyrek CT, et al. Structural studies on some dithiophosphonato complexes of Ni(II), Cd(II), Hg(II) and theoretical studies on a dithiophosphonato Ni(II) complex using density functional theory. *J Mol Struct*. 2015;1099:490-501.
- 26. Chakravarty M, Pailloux S, Ouizem S, et al. Synthesis and metal coordination chemistry of (phenyl)(pyridin-2-ylmethyl)phosphinodithioic acid, [2-C5H4N]CH2P(S)(SH)(Ph). *Polyhedron*. 2012;33:327-335.



Degradation of Chrysoidine Y Dye with Sulphite Ion in Aqueous Acidic Phase using Kinetic **Method of Analysis**

Patricia Ese UMORU¹ Ikechukwu Ugbaga NKOLE 2 (ib



Kinetik Analiz Yöntemi Kullanılarak Sulu Asidik Fazda Sülfit İyonlu Krizoidin Y Boyasının Bozunması

¹Department of Chemistry, Faculty of Science, Nigerian Defence Academy, Kaduna, Nigeria

²Basic Science Unit, Wigwe University, Isiokpo, Nigeria



Geliş Tarihi/Received 11 01 2025 Kabul Tarihi/Accepted 19.03.2025 Yayın Tarihi/Publication 21.05.2025 Date

Sorumlu Yazar/Corresponding author: Patricia Ese Umoru,

E-mail: peumoru@nda.edu.ng

Cite this article: Umoru PE, Nkole IU. Degradation of Chrysoidine Y Dye with Sulphite Ion in Aqueous Acidic Phase using Kinetic Method of Analysis . J Ata-Chem. 2025;5(1): 10-19.



Content of this journal is licensed under a Creative Commons Attribution-Noncommercial 4.0 International License.

ABSTRACT

Chrysoidine Y dye (CYD) is harmful to aquatic species and human beings, which has the tendency to induce cancer and mutation to living cells. Its degradation is key in creating a healthy environment and curbing pollution. Hence, a stoichiometric method is used to study its degradation with a pool of sulphite ions (SO₃²⁻), under a constant ionic strength, $[H^{+}]$, and 449 nm wavelength. The stoichiometry is observed to be 1:1 for CYD: SO_{3}^{2-} , which results in the formation of aniline and sulphonic acid as the main products of the degradation. The reaction is first-order with respect to CYD, first-order with respect to SO₃²-, and a second-order-overall. Increase in the proton concentration impacts positively on the reaction rate of CYD degradation. Negative salt effect is observed as the dilapidation rate of the dye drops. Occurrence of counter ion catalysis is pronounced with large appreciable rate. The participation of a firm intermediate molecule is negative as revealed by the Spectroscopic Scanning Technique (SST) and Michaelis Menten's Type Plot (MMTP), which cancels the inner-sphere mechanism expectancy. The degradation of the dye was successfully carried out and the reaction points to the outer-sphere mechanism

Keywords: Degradation, Chrysoidine Y, Sulphite ion, Acidic phase, Kinetics

ÖZ

Krizoidin Y boyası (CYD), kansere ve canlı hücrelerde mutasyona neden olma eğiliminde olan su canlıları ve insanlar için zararlıdır. Bozunumu sağlıklı bir çevre yaratmada ve kirliliği azaltmada anahtar rol oynar. Bu nedenle, sabit iyonik güç [H⁺] ve 449 nm dalga boyu altında bir sülfit iyonları havuzunda (SO₃²⁻) bozunmasını incelemek için stokiyometrik bir yöntem kullanılır. Stokiyometrik oranın CYD: SO₃²⁻ için 1:1 olduğu gözlemlenir ve bu da bozunmanın ana ürünleri olarak anilin ve sülfonik asit oluşumuyla sonuçlanır. Tepkime CYD açısından birinci dereceden, SO_3^{2-} açısından birinci dereceden ve genel olarak ikinci derecedendir. Proton konsantrasyonundaki artış, CYD bozunmasının reaksiyon hızını olumlu yönde etkiler. Boyanın bozulma hızı düştükçe negatif tuz etkisi gözlemlenir. Karşı iyon katalizinin oluşumu büyük ve belirgin bir hızla belirgindir. Spektroskopik Tarama Tekniği (SST) ve Michaelis Menten Tip Grafiği (MMTP) tarafından ortaya konulduğu gibi, sağlam bir ara molekülün katılımı negatiftir ve bu da iç küre mekanizması beklentisini iptal eder. Boyanın bozunması başarıyla gerçekleştirildi ve reaksiyon dış küre mekanizmasına işaret etmektedir.

Anahtar Kelimeler: Bozunma, Krizoidin Y, Sülfit iyonu, Asidik faz, Kinetik

INTRODUCTION

Chrysoidine Y dye here after referred to as (CYD) is an azo-dye with nitrogen-nitrogen double bond functional group that is frequently used in the leather, polymer, food, and cosmetic industries.1 The dye is well known to be resistant to biodegradation as well photo-stability. It is reported to be carcinogenic, mutagenic, and has toxicity which has traits to the environment and human system.² CYD removal has been studied with biosorbents produced from row-cork and cork stocked in Ca-alginate bead.³ It has been demonstrated that oral administration of Chrysoidine Y results in liver-cell adenomas, carcinomas and leukemia in animals.⁴ Modified Hummers and co-precipitation approach was employed by Hao et al. 5 to study the removal of CYD with nano-almagamated iron oxidegraphene oxide, as adsorbent. The process was pseudosecond-order compliance and was largely pH dependent, which is in collaboration with the report of Gote et al. 6 where the help of hydrogen peroxide and nickel-iron oxide catalyst, a sono-catalytic method was used to degrade chrysoidine R Also, the rate removal was chemi-sorption influenced, which is a pointer that chemical process can be a better means of degrading CYD dyes. Ensuring a clean environment Mittal and co-scientists⁷ studied the removal and recovery of CYD dye with agricultural wastes (bottom ash and oil-free soya). The impact of the tested parameters (pH, contact time, particle size, and adsorbent concentration) had a significant effect on the removal process of the dye. The use of CYD for staining tissues and in textiles can course pollution in water bodies as well as humans and its environment.

Chemical-coagulation approach was deployed by Mariyam and co-workers⁸ to study the removal of chrysoidine R, an analogue of CYD Y dye, on an organometal framework. The impact of $[H_3O^+]$ and adsorption time were laudable with the implication of chemi-sorption as the rate controlling route. Ashraf et al., ⁹ contributed to the removal studies of CYD with sawdust and the striking observation was high rate of CYD adsorption in pseudo-second-order fashion. The submission buttressed the far fetching need for chemical degradation of CYD to ensure eco-friendly system.

Sulphite ion is used to reduce chromium (VI) to chromium (III), making it less toxic. ¹⁰ Sulphite ion acts as an antioxidant and preservative in foods and beverages to prevent browning and spoilage. ¹¹ In photographic processing, sulphite reduce silver halides thereby helping to develop photographs. Furthermore, it is used in organic synthesis to reduce various functional groups, including ketones and aldehydes. Sulphite ion is equally employed in the pulp and paper industry to bleach wood pulp without

the use of chlorine. In dyeing processes, sulphite can help reduce certain dyes and modify their properties. ¹²⁻¹⁵

The aim of the study is to contribute to clean environment by exploiting the redox potential species, sulphite ion in the degradation of CYD and explaining its mechanistic pathway.

Much work has not been reported on the degradation of CYD which has prompted this research to see how CYD can be degraded to a less harmful compound.

This study is therefore carried out to see how CYD can be degraded using kinetic method of analysis due to the fact that chemical process is a better means of degrading CYD and this is not well documented in literature.

MATERIALS AND METHODS

Materials

Chrysoidine Y dye and sodium sulphite were obtained from Sigma-Aldrich, Germany. Sodium chloride (BDH, UK) was used to keep the reaction's salt effect constant. Magnesium chloride, potassium chloride, and sodium nitrate (May and Baker, Nigeria) were used to ascertain the effect of counter ions on the reaction rate. Hydrochloric acid (BDH, UK) was used to study the effect of [H⁺] on the rate of reaction. Acetone (May and Baker, Nigeria) was used to investigate the effect of solvent polarity (dielectric constant) on the reaction mixture. Bromine water, carbon disulphide, and sodium bicarbonate (BDH, UK) was used for product analysis. Acrylamide with methanol (May and Baker, Nigeria) was used to check the participation of unstable atoms in the reaction. Kinetic investigations were performed with a UV/Visible 752s) spectrophotometer (Spectrum Lab and characterisation of reaction products were carried out qualitatively.

Methods

Maximum Absorbance Determination: The maximum absorbance was determined by running a $0.1~\text{mol}~\text{dm}^{-3}$ solution in a UV/Visible spectrophotometer in the range of 200 - $800~\text{nm}.^9$

Stoichiometry and product determination: The stoichiometry of the reaction was determined spectrophotometrically using the mole ratio method under the reaction conditions [CYD] = 1.0×10^{-4} mol dm⁻³, [SO₃²⁻] = $(0.2-1.6) \times 10^{-4}$ mol dm⁻³, [H⁺] = 1×10^{-2} mol dm⁻³, I = 1.0 mol dm⁻³, T = 30 ± 1 °C and λ_{max} = 449 nm. For a series of solutions containing constant [CYD], the [SO₃²⁻] (where [] symbolizes concentration) was varied and the absorbance of the reaction mixtures were measured for an interval of eight hours after the initial measurement before arriving at

constant absorbance after twenty hours. 16-20

The products of the degradation were elucidated by the addition of six drops of bromine water to the product mixture and four drops of carbon disulphide solution. Also, eight drops of sodium bicarbonate solution were added in a separate portion.

Kinetic examination: The reaction order was determined by observing the bleaching of the reaction system as the reaction proceed at a maximum absorbance = 449 nm. The process was done using pseudo-first-order settings with the least concentration of SO_3^{2-} at 200-fold in excess over [CYD] and constant ionic strength of 1.0 mol dm⁻³. A graph of absorbance (A) against time (s) was done and the observed rate constants, k_1 were obtained as the gradients of the graphs represented by equation 1: $^{21-24}$

$$A_t/A_0 = \exp(-k_1 t)$$

where A_t and A_0 are the absorbance at the time t, and 0, respectively, k_1 is the observed rate constant and t is the time (seconds). The second-order rate constants, k_2 were determined from equation 2:

$$k_2 = k_1/[SO_3^{2-}]$$
 2

The effect of hydrogen ion concentration was determined at the range of 0.5-3.0 mol dm⁻³, the salt effect of the reaction medium within the range of 0.5 - 3.0 mol dm⁻³, and the solvent polarity was varied by the addition of acetone (0.5 - 3.0) cm³ at constant concentrations of the reactants and temperature $30 \pm 1^{\circ}\text{C}.^{22\text{-}27}$

The effect of added counter ions was investigated under a constant concentration of CYD, SO_3^{2-} , ionic strength, and at [ion] = $0.5-3.0\times10^{-3}$ mol dm⁻³. ²⁸⁻³⁰

The investigation of the existence of unstable atoms in the reaction mixture was carried out by adding 0.2 cm³ of acrylamide solution to an incompletely reacted CYD-SO₃²⁻ mixture and excess of methanol. ³¹⁻³³

The intermediate complex was examined spectroscopically by scanning the partially reacted mixture at wavelength 200–800 nm, and applying the Michaelis–Menten's plot of k_1^{-1} against $[SO_3^{2-}]^{-1}$. $^{34-36}$

RESULTS

Maximum Absorbance of CYD: The maximum absorbance of CYD is observed at 449 nm.

Stoichiometry and Product Determination: A mole ratio of 1:2 (CYD: SO_3^{2-}) is obtained for the reaction between CYD: SO_3^{2-} (Figure 1). Indicative of 4e- contribution

from the sulphite ion for the breakdown of a mole of CYD and it is buttressed by equation 3.

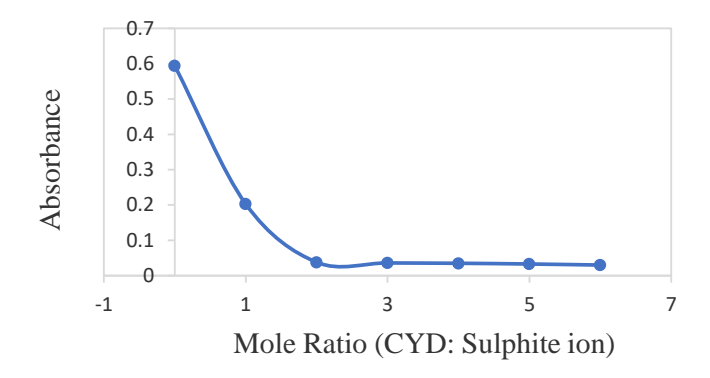


Figure 1: Plot of absorbance versus [SO₃²⁻] for the determination of the stoichiometry of CYD - SO₃²⁻ System.

On the addition of six drops of bromine water to the product mixture, the mixture turned to a white precipitate, indicating the deposit of aniline, which was confirmed by a mustard oil smell when four drops of carbon disulphide solution was added to a separate portion of the product mixture. Also, the sulphonic acid group was confirmed by the release of effervescence in the form of bubbles on the addition of eight drops of sodium bicarbonate solution to a portion of the product mixture.

Kinetic Examination

The reaction resulted in a first order with respect to the [CYD] due to consecutive linearity of the graphs of log $(A_t - A_\infty)$ against time and a typical one is shown in Figure 2, and first - order with respect to the concentration of SO_3^{2-} as proven by the logarithmic plot of k_1 against $[SO_3^{2-}]$ that is one dimensional with a slope 0.9971 and a correlation coefficient $R^2 = 0.9995$ (Figure 3), which is reinforced by the consistency of the k_2 in Table 1.

The rate of the reaction is positively affected as the concentration of acid is increased for CYD - SO₃²⁻. This result is contrary to the report of Edokpayi et al.³⁷; Imam et al.³⁸ where increase in [H⁺] had no effect on rate of reaction between indigo carmine and sulphite ion; malachite green with sulphite ion systems, respectively.

$$N=N$$
 $+2SO_3^{2-}$
 NH_2
 $+H_2+N_2$
 SO_3H
 $+H_2+N_2$
 SO_3H

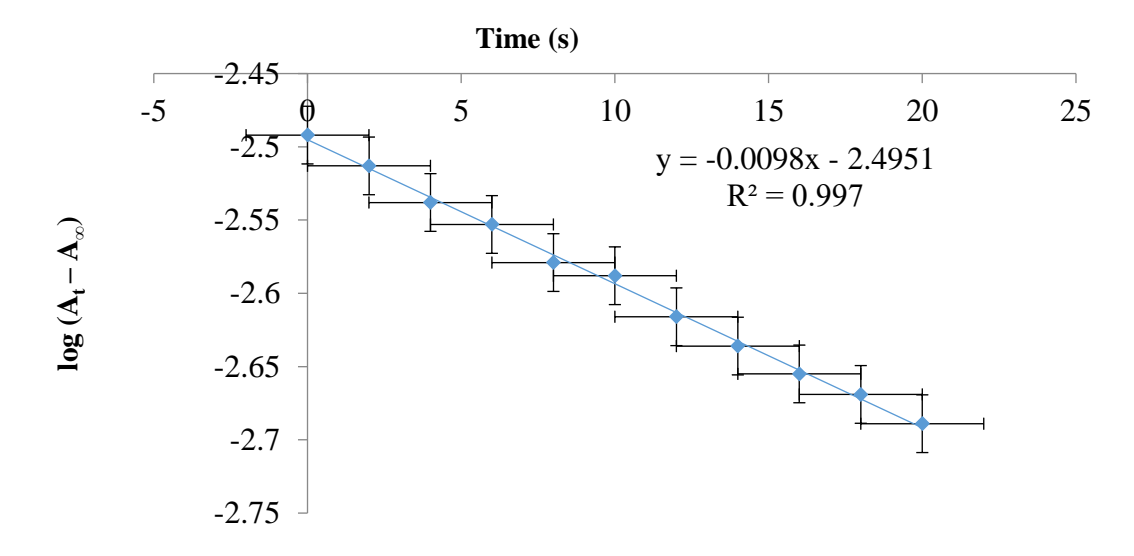


Figure 2: Graph of the logarithm plot of $(A_t - A_{\infty})$ against time for the degradation of CYD by $SO_3^{2^-}$. [CYD] = 1.0×10^{-4} mol dm⁻³, [SO₃²⁻] = $(2.0 - 10) \times 10^{-2}$ mol dm⁻³, [H⁺] = 1×10^{-2} mol dm⁻³, I = 1.0 mol dm⁻³, T = 30 ± 1 °C, and λ_{max} = 449 nm.

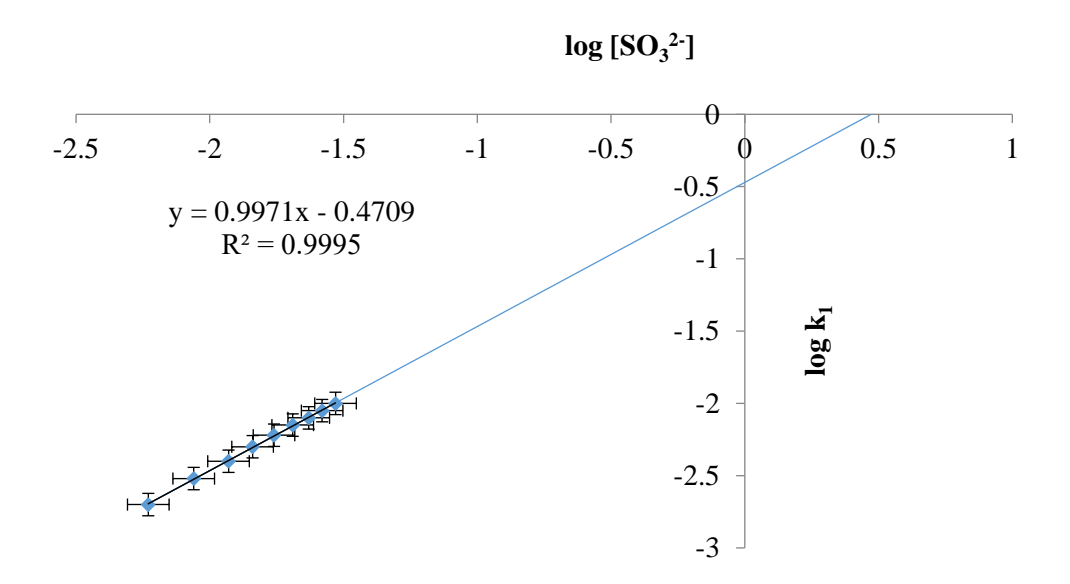


Figure 3: Logarithm plot of k_1 against $[SO_3^{2-}]$ for the degradation of CYD by SO_3^{2-} . $[CYD] = 1.0 \times 10^{-4}$ mol dm⁻³, $[SO_3^{2-}] = (2.0 - 10) \times 10^{-2}$ mol dm⁻³, $[H^+] = 1 \times 10^{-2}$ mol dm⁻³, I = 1.0 mol dm⁻³, $I = 30 \pm 1$ °C, and $\lambda_{max} = 449$ nm.

Table 1: Kinetics constant for the degradation of CYD by $SO_3^{2^-}$. [CYD] = 1.0×10^{-4} mol dm⁻³, [$SO_3^{2^-}$] = $(2.0 - 10) \times 10^{-2}$ mol dm⁻³, T = 30 ± 1 °C, and λ_{max} = 449 nm.

10 ² [SO ₃ ²⁻],	l,	10²[H+],	10 ² k ₁ ,	k ₂ ,
mol dm ⁻³	mol dm ⁻³	mol dm ⁻³	S ⁻¹	dm³ mol ⁻¹ s ⁻¹
2.0	1.0	1.0	2.26	1.13
3.0	1.0	1.0	3.40	1.13
4.0	1.0	1.0	4.60	1.15
5.0	1.0	1.0	5.70	1.14
6.0	1.0	1.0	6.90	1.15
7.0	1.0	1.0	8.00	1.14
8.0	1.0	1.0	8.90	1.11
9.0	1.0	1.0	10.00	1.11
10.0	1.0	1.0	11.00	1.10
3.0	1.0	0.5	3.40	1.13
3.0	1.0	1.0	3.42	1.14
3.0	1.0	1.5	3.64	1.21
3.0	1.0	2.0	4.10	1.37
3.0	1.0	2.5	4.30	1.43
3.0	1.0	3.0	5.30	1.77
3.0	0.5	1.0	3.67	1.22
3.0	1.0	1.0	3.42	1.14
3.0	1.5	1.0	3.22	1.07
3.0	2.0	1.0	3.05	1.02
3.0	2.5	1.0	2.89	0.96
3.0	3.0	1.0	2.71	0.90

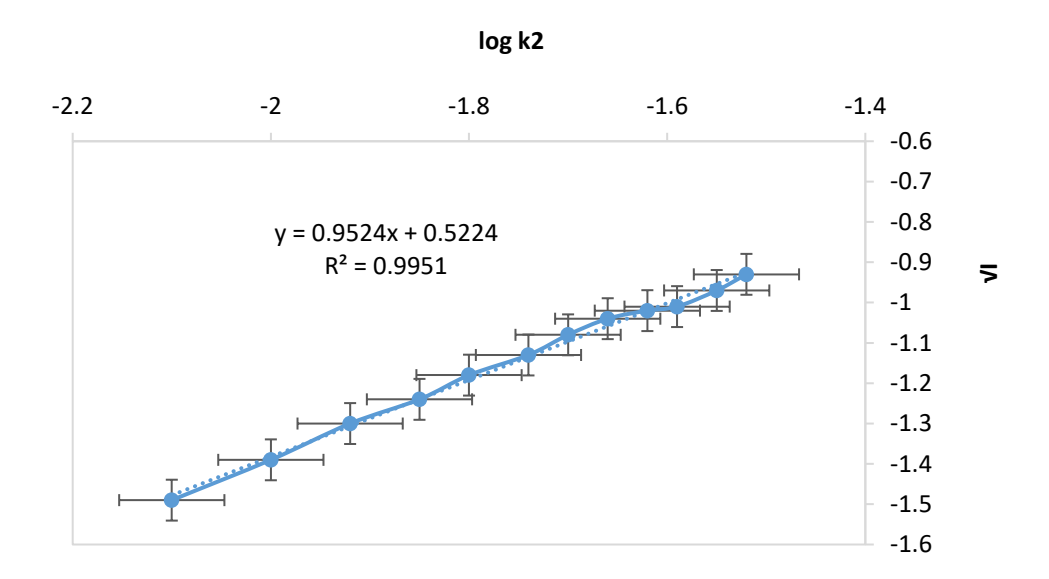


Figure 4: Graph of salt effect of k_2 versus VI for the degradation of CYD by $SO_3^{2^-}$. [CYD] = 1.0×10^{-4} mol dm⁻³, [SO₃²⁻] = 3.0×10^{-2} mol dm⁻³, [H⁺] = 1.0×10^{-2} mol dm⁻³, T = 30 ± 1 °C, and λ_{max} = 449 nm.

The overall rate equation can be represented by equations 4 as follows:

$$-\frac{d[CYD]}{dt} = [CYD][SO_3^{2-}]$$

A negative salt effect is observed in the redox reaction as the rate of reaction is found to decrease with increase in the ionic strength of the reaction medium (Figure 4). The observed slope of less than one could be due to formation of ion – pair during the reaction. The negative Brønsted – Debye salt effect observed indicates that the species at the activated complex are of unlike charges.

The effect of change in dielectric constant is studied by using a binary solvent mixture of water and acetone (0.5 - 3.0) cm³. It is observed that as the concentration of acetone increased, the rate of reaction increased for CYD - SO_3^2 (Table 2).

Added counter ions $(Mg^{2+}, K^+, and NO_3^-)$ increased rate of reaction as the concentration increased (Table 3). Ibrahim et al. ³⁹, Abdulsalam et al. ⁴⁰, Oladunni et al. ⁴¹ reported that added ions are expected to catalyse reactions occurring by the outer-sphere mechanism. As such, this reaction is most probably in the favour of an outer – sphere mechanism.

The addition of 2 cm³ acrylamide solution to the partially reduced CYD mixture shows no gel formation even in large excess of methanol, suggesting the probable absence of free radicals in the reaction systems.

The plot of k_1^{-1} versus $[SO_3^{2-}]^{-1}$ gives a straight line, which passes through the origin (Figure 5). This suggests absence of intermediate complex formation prior to redox reaction. In addition, the result of the spectroscopic study indicates no significant shift from the absorption maxima of λ_{max} = 449 nm. This suggests the absence of the formation of an intermediate complex in the reaction.

Table 2: Effect of system permittivity on the reaction rate for the degradation of CYD by SO_3^{2-} . [CYD] = 1.0×10^{-4} mol dm⁻³, [SO₃²⁻] = 3.0×10^{-2} mol dm⁻³, [H⁺] = 1.0×10^{-2} mol dm⁻³, I = 1.0×10^{-2} mol dm⁻³, T = 30 ± 1 °C, and $\lambda_{max} = 449$ nm.

Acetone-H ₂ O (cm ³)	10 ¹ k ₁ , s ⁻¹	k ₂ , dm³ mol ⁻¹ s ⁻¹
0.5	7.83	2.61
1.0	8.73	2.91
1.5	9.65	3.22
2.0	10.57	3.52
2.5	11.56	3.85
3.0	12.43	4.14

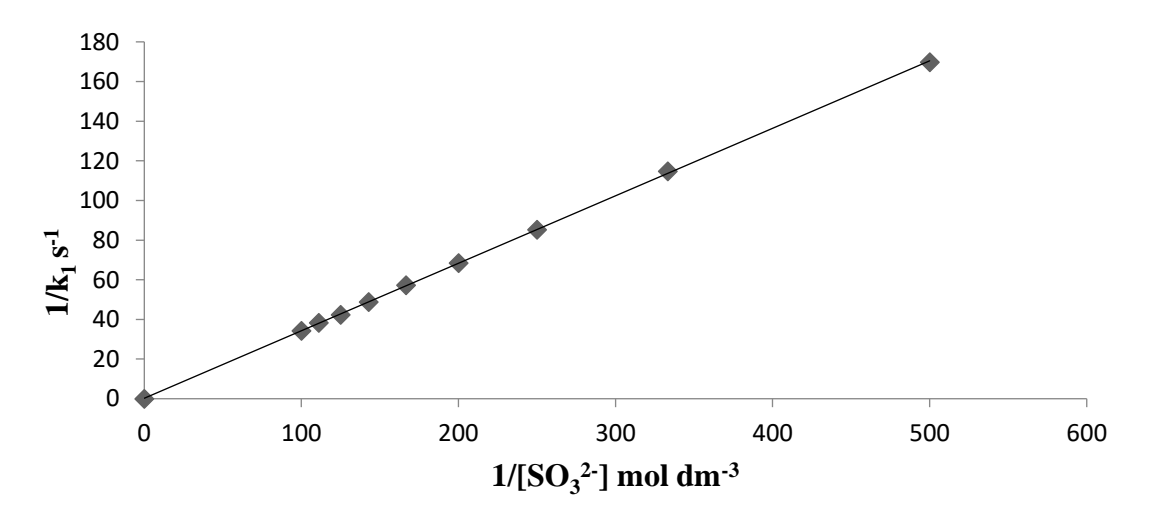


Figure 5: Plot of k_1^{-1} versus $[SO_3^{2-}]^{-1}$ for the degradation of CYD by SO_3^{2-} .

Table 3: Effect of counter ions on the reaction rate for the degradation of CYD by SO_3^{2-} [CYD] = 1.0×10^{-4} mol dm⁻³, [SO_3^{2-}] = 3.0×10^{-2} mol dm⁻³, [H⁺] = 1.0×10^{-2} mol dm⁻³, I = 1.0×10^{-2} mol dm⁻³, T = 30 ± 1 °C and λ_{max} = 449 nm.

Ion	10 ³ [lon], mol dm ⁻³	10 ³ k ₁ , s ⁻¹	k ₂ , dm ³ mol ⁻¹ s ⁻¹
	0.5	7.59	2.53
Mg ²⁺	1.0	8.74	2.91
	1.5	9.89	3.30
	2.0	11.04	3.68
	2.5	12.19	4.06
	3.0	13.34	4.45
	0.5	7.74	2.58
K ⁺	1.0	8.73	2.91
	1.5	9.72	3.24
	2.0	10.70	3.57
	2.5	11.67	3.89
	3.0	12.65	4.22
	0.5	7.29	2.43
	1.0	8.73	2.91
NO ₃ -		10.18	3.39
		11.63	3.88
		13.05	4.35
		14.49	4.83

 NH_2

Reaction Mechanism:

 NH_2

N=N,
$$H_{2}$$
 HCI (5)

NH₂

N=N, H_{3}^{+}

NH₂

NH₃
 H_{3}^{+}

NH₃
 H_{4}^{+}

NH₃

NH₃
 H_{4}^{+}

NH₂
 H_{2}^{+}

NH₂
 H_{3}^{+}
 H_{2}^{+}
 H_{2}^{+}
 H_{2}^{+}
 H_{2}^{+}
 H_{2}^{+}
 H_{3}^{-}
 H_{2}^{+}
 H_{3}^{+}
 H_{3}^{+}
 H_{3}^{+}
 H_{3}^{+}
 H_{4}^{-}
 H_{2}^{+}
 H_{3}^{-}
 H_{2}^{-}
 H_{3}^{-}
 H_{3}^{-}
 H_{4}^{-}
 H_{2}^{-}
 H_{3}^{-}
 H_{3}^{-}
 H_{4}^{-}
 H_{3}^{-}
 H_{4}^{-}
 H_{3}^{-}
 H_{4}^{-}
 H_{3}^{-}
 H_{4}^{-}
 H_{3}^{-}
 H_{4}^{-}
 H_{3}^{-}
 H_{4}^{-}
 H_{4}^{-}
 H_{4}^{-}
 H_{4}^{-}
 H_{4}^{-}
 H_{4}^{-}
 H_{4}^{-}
 H_{4}^{-}
 H_{4}^{-}
 H_{4}^{-}
 H_{4}^{-}
 H_{4}^{-}
 H_{4}^{-}
 H_{4}^{-}
 H_{4}^{-}
 H_{4}^{-}
 H_{4}^{-}
 H_{4}^{-}
 H_{4}^{-}
 H_{4}^{-}
 H_{4}^{-}
 H_{4}^{-}
 H_{4}^{-}
 H_{4}^{-}
 H_{4}^{-}
 H_{4}^{-}
 H_{4}^{-}
 H_{4}^{-}
 H_{4}^{-}
 H_{4}^{-}
 H_{4}^{-}
 H_{4}^{-}
 H_{4}^{-}
 H_{4}^{-}
 H_{4}^{-}
 H_{4}^{-}
 H_{4}^{-}
 H_{4}^{-}
 H_{4}^{-}
 H_{4}^{-}
 H_{4}^{-}
 H_{4}^{-}
 H_{4}^{-}
 H_{4}^{-}
 H_{4}^{-}
 H_{4}^{-}
 H_{4}^{-}
 H_{4}^{-}
 H_{4}^{-}
 H_{4}^{-}
 H_{4}^{-}
 H_{4}^{-}
 H_{4}^{-}
 H_{4}^{-}
 H_{4}^{-}
 H_{4}^{-}
 H_{4}^{-}
 H_{4}^{-}
 H_{4}^{-}
 H_{4}^{-}
 H_{4}^{-}
 H_{4}^{-}
 H_{4}^{-}
 H_{4}^{-}
 H_{4}^{-}
 H_{4}^{-}
 H_{4}^{-}
 H_{4}^{-}
 H_{4}^{-}
 H_{4}^{-}
 H_{4}^{-}
 H_{4}^{-}
 H_{4}^{-}
 H_{4}^{-}
 H_{4}^{-}
 H_{4}^{-}
 H_{4}^{-}
 H_{4}^{-}
 H_{4}^{-}
 H_{4}^{-}
 H_{4}^{-}
 H_{4}^{-}
 H_{4}^{-}
 H_{4}^{-}
 H_{4}^{-}
 H_{4}^{-}
 H_{4}^{-}
 H_{4}^{-}
 H_{4}^{-}
 H_{4}^{-}
 H_{4}^{-}
 H_{4}^{-}
 H_{4}^{-}
 H_{4}^{-}
 H_{4}^{-}
 H_{4}^{-}
 H_{4}^{-}
 H_{4}^{-}
 H_{4}^{-}
 H_{4}^{-}
 H_{4}^{-}
 H_{4}^{-}
 H_{4}^{-}
 H_{4}^{-}
 H_{4}^{-}
 H_{4}^{-}
 H_{4}^{-}
 H_{4}^{-}
 H_{4}^{-}
 H_{4}^{-}
 H_{4}^{-}
 H_{4}^{-}
 H_{4}^{-}
 H_{4}^{-}

Following the outcome of the kinetic evidence from the effect of ionic strength, acid, added ions, MMTP, and absence of stable and detectable free-radicals, an outersphere mechanism (equation 5 - 7) is considered.

DISCUSSION

The study of degradation of CYD with SO_3^{2-} ion using a kinetic method of analysis portrays a sustainable and efficient approach in determining the pathway of the degradation with rate input.

A maximum absorbance of 449 nm was obtained for this research, Ashaf et al. 9 reported the same wavelength and 452 nm was reported by Gote et al. 6 for sonocatalytic degradation of chrysoidine R dye, an analogue of CYD, using ultrasonically synthesized NiFe₂O₄ catalyst.

A contrary stoichiometry of 2: 1 was observed for the reaction between $[Mn(cydta)(OH,]^{-}$ and SO_3^{2-} as reported by Chandrawat et al.⁴² for the Kinetics and mechanism of the oxidation of the sulphite ion by Mn(III)-cydta complex ion .

The order of the degradation is first order with respect to the concentrations of the two reacting species (CYD and ${\rm SO_3}^{2-}$) indicating second- order kinetics. A similar order was observed for the degradation of chrysoidin R dye⁶.

Acid medium increased the rate of reaction positively which is contrary with the result of ^{37,38} but is however in agreement with the report of.⁴²

The ionic strength accounts opposite charged species interaction which is also contrary to the report of ⁴² where similar charges are in operation during the redox reaction.

Free radicals are absent in the process added added ions had effect on the rate of reactions. Thus, the result is suggestive of an outer-sphere mechanism degradation process. These results are contrary to the results reported by Umoru, Babatunde 2019^{43} for the Kinetics and Mechanism of the Oxidation of Sulphite Ion by Di- μ -oxo-tetrakis (2, 2' bipyridine)-Dimanganese (III, IV) Perchloratein Aqueous Acidic Medium.

Hakem Değerlendirmesi: Dış bağımsız.

Yazar Katkıları: Kaynaklar, Veri Toplama ve/veya İşleme, Analiz ve/veya Yorumlama, Literatür: Patricia Ese Umoru. Kavram, Tasarım, Denetleme, Kaynaklar, Literatür Araştırması, El Yazması, Eleştirel İnceleme: Ikechukwu Nkoli.

Teşekkür: Yazarlar, çalışmaya sağladıkları destek için Nijerya Savunma Akademisi Kimya Bölümü ve Wigwe Üniversitesi, Isiokpo, Nijerya, Bilim ve Bilgisayar Fakültesi'ne teşekkür etmek isterler.

Çıkar Çatışması: Yazarlar, çıkar çatışması olmadığını beyan etmiştir. **Etik Komite Onayı:** Bu çalışma için etik kurul onayı gerekmemektedir. **Finansal Destek:** Bu çalışma tüm yazarlar tarafından finanse edilmiştir.

Peer-review: Externally peer-reviewed.

Author Contributions: Resources, Data Collection and/or Processing, Analysis and/or Interpretation, Literature: Patricia Ese Umoru. Concept, Design, Supervision, Resources, Literature Search, Writing Manuscript, Critical Review: Ikechukwu Nkoli

Acknowledgement: The authors wish to acknowledge the Department of Chemistry, Nigerian Defence Academy and the College of Science and Computing, Wigwe University, Isiokpo, Nigeria for their support in the study.

Conflict of Interest: The authors have no conflicts of interest to declare. **Ethics Committee Approval:** Ethics committee approval is not required for this study.

Financial Disclosure: This study was financed by all the authors.

REFERENCES

- 1. Shammala FA, Chiswell B. Removal of Chrysoidine Y from water by graphene-based nanocomposite derivatives with magnetic chitosan nanocomposite. *Intl J Appl Pharm Sci.* 2019;4:17-33.
- 2. Hou J, Yun J, Jang W, Kim J, Byun H. Polyacrylonitrile nanofiber membranes incorporated with large reduced graphene oxide content in situ. *J Mater Sci.* 2021;56:18508-18521.
- 3. Nurchi VM, Crespo-Alonso, Beisuz R, et al. Sorption of chrysoidine by row cork and cork entrapped in calcium alginate beads. *Arabian J Chem*. 2014;7:133-138.
- 4. International Agency for Research on Cancer (IARC). (1975). *IARC Monographs on the Evaluation of Carcinogenic Risk of Chemicals to Man*, Volume 8: Some Aromatic Azo Compounds, pp. 91–96. Lyon, France: IARC. ISBN 978-92-832-1208-9.
- Hao Y, Wang Z, Gou J, Dong S. Highly efficient adsorption and removal of Chrysoidine Y from aqueous solution by magnetic graphene oxide Nanocomposite.
 2015;http://dx.doi.org/10.1016/j.arabjc.2015.07.01
- 6. Gote YM, Sinhmar PS, Gogate PR. Sonocatalytic degradation of chrysoidine R dye using ultrasonically synthesized NiFe₂O₄ catalyst. *Catalysts*. 2023;13:597.
- 7. Mittal A, Mittal J, Malviya A, Gupta VK. Removal and recovery of Chrysoidine Y from aqueous solutions by

- waste materials. *J Colloid Interface Sci.* 2010;344:497-507.
- Mariyam A, Mittal J, Sakina F, Baker RT, Sharma A, K. Adsorption behaviour of Chrysoidine R dye on a metal/halide-free variant of ordered mesoporous carbon. *Desal Water Treatment*. 2021;223:425-433.
- 9. Ashraf MW, Abulibdeh N, Salam A. Adsorption studies of textile dye (chrysoidine) from aqueous solutions using activated sawdust. *Intl J Chem Eng.* 2019;1-8.
- 10. Beukes JP, Pienaar JJ, Lachmann G, Giesekke EW. The reduction of hexavalent chromium by sulphite in water-waste. *Water SA*. 1999;25:363-370.
- 11. Hamid AA, Risikat A, Sururah A. Food: its preservations, additives and applications. *Intl J Chem Biochem Sci.* 2012;1:36-47.
- 12. Vally H, Misso NLA. Adverse reactions to the sulphite additives. *Gastroenterol Hepatol Bed Bench*. 2012;5:16-23.
- 13. Zhao D, Yang C, Xiao C, et al. Quality evaluation and identification of *Houttuynia cordata* bleached with sodium metabisulphite based on whole spectrum metabololmics. *Food Chem X*. 2024;14:101463.
- 14. Wairimu NW, Wairagu P, Chepukosi KW, et al. Sodium metabisulphte-induced hematotoxicity, oxidative stress, and organ damage ameliorated by standardized *Ginkgo biloba* in mice. *J Toxicol*. 2023;10:7058016.
- Irwin SV, Fisher P, Graham E, Malek A, Robidoux A. Sulphite inhibit the growth of four species of beneficial gut bacteria at concentrations regarded as safe for food. *Plos One*. 2017;12:0186629.
- 16. Nkole IU, Osunkwo CR, Onu AD, Idris SO. Kinetics and mechanism of the reduction of n-(2hydroxyethyl)ethylenediaminetriacetateiron(III) complex by thioglycol in bicarbonate buffer medium. *Intl J Adv Chem*. 2018;6:102–107.
- 17. Idris SO, Tanimu A, Iyun JF, Mohammed Y. Kinetics and mechanism of the reaction of malachite green and dithionite ion. *Intl Res J Pure Appl Chem*. 2015;5:177–184.
- Arthur DE, Nkole IU, Osunkwo CR. Electron transfer reaction of tris(1,10-phenanthroline)cobalt(III) complex and iodide ion in an aqueous acidic

- medium. Chem Afr. 2020;4:63-69.
- 19. Umoru PE, Faruruwa MD. Kinetic analysis of the oxidation of nitrate ion by methylthioninium chloride in acid medium. *J Appl Sci Environ Manage*. 2014;18:460-466.
- 20. Onu AD, Iyun JF, Idris SO. Kinetics and stoichiometry of the reduction of hydrogen peroxide by an aminocarboxlactocobaltate(II) complex in aqueous medium. *Open J Inorg Chem*. 2015;5:75–82.
- 21. Sawicki E, Noe JL, Fox FT. Spot test detection and colorimetric dterminations of aniline, naphthylamine, and anthramine derivatives with 4-azobenzenediazonium fluoborate. *Talanta*. 1961;8:257-264.
- 22. Bruzzoniti MC, De Carlo RM, Sarzanini A. Determination of sulfonic acids and alkylsulfates by ion chromatography in water. *Talanta*. 2007;75:734-739.
- 23. Nkole IU, Idris SO, Abdulkadir I, Onu AD. Cationic surfactant-based catalysis on the oxidation of glutamic acid by bis-(2-pyridinealdoximato)dioxomolydate(IV) complex. *Catal. Lett.* 2023;153:1-10.
- 24. Shanmugaprabha T, Selvakumar K, Rajasekaran K, Sami P. A kinetic study of the oxidations of 2-mercaptoethanol and 2-mercaptoethylamine by heteropoly 11-tungsto-1-vanadophosphate in aqueous acidic medium. *Trans Met Chem*. 2016;41:77–85.
- 25. Osunkwo CR, Nkole IU, Onu AD, Idris SO. Electron transfer reaction of tris-(1,10-phenanthroline)cobalt(III) complex $[Co(phen)_3]^{3+}$ and thiosulphate ion $(S_2O_3^{2-})$ in an aqueous acidic medium. *Intl J Adv Chem.* 2018;6:121–126.
- Nkole IU, Idris SO, Abdulkadir I, Onu AD. Effect of surfactant micellization on the oxidation of mercaptobenzothiazole by bioinorganic molybdenum complex. Results Chem. 2022;2:100616.
- 27. Myek B, Idris SO, Onu AD, Yakubu MK. Kinetics and mechanism of the redox reaction of orange II with thiosulphate ion in aqueous acid. *Sci World J.* 2020;15:108-111.
- 28. Ukoha PO, Atiga S, Ujam OT, Asegbeloyin JN, Okpareke OC, Okereke SOE. Kinetics and mechanism

- of electron transfer reaction of an adipato bridged iron(III)-salen complex with dithionite ion in perchloric acid medium. *Croatica Chemica Acta*. 2015;88:259-266.
- 29. Nkole IU, Idris SO, Abdulkadir I, Onu AD. Redox reaction of bis-(2-pyridinealdoximato)dioxomolybdate(IV) complex with thiosulphate ion in aqueous acidic and surfactant media. *Inorg Chem Comm.* 2022;140:109468.
- 30. Umoru PE, Nkole IU, Ezeh TT. Degradation of indigo carmine dye with peroxydisulphate ion in aqueous sulphuric acid phase: kinetic study. *Intl J Chem Kinet*. 2024;56:1-8.
- 31. Ibrahim I, Idris SO, Abdulkadir I, Onu AD. Premicellar effects on the reduction of n,n'-phenylenebis(salicylideneimianto)iron(III) by thioglycolic acid: kinetic study and mechanism. *J Disper Sci Technol*. 2023;45:1634-1645.
- 32. Atiga S, Ukoha PO, Ujam OT, Okpareke OC. Kinetics and mechanism of the reduction of μ -adi-di(n,n'-bis-(salicylideneethylenediaminatoiron(III))) complex with dithionate ion. *Transit Metal Chem*. 2014;39:189-194.
- 33. Nkole IU, Idris SO, Abdulkadir I, Onu AD. Oxidation of aspartic acid with molybdenum-oxime-ligand framework in acidified-aqua and interfacial active media: Menger-Portnoy kinetic model. *Inorg Chem Comm.* 2024;161:111979.
- 34. Tang JY. On the relationships between the Michaelis-Menten kinetics, reverse Michaelis-Menten kinetics, equilibrium chemistry approximation kinetics, and quadratic kinetics. Geosci Model Dev. 2015;8:3823-3835.
- 35. Srinivasan B. A guide to the Michaelis-Menten equation: steady state and beyond. *FEBS J.* 2021;289:6086-6098.
- 36. Nkole IU, Imam M, Arthur DE. Oxidation of glyoxal with the Mo-oxime complex in a benzalkonium chloride interface: Raghavan and Srinivasan kinetic model. *Inorg Chem Comm*. 2024;170:113524.
- 37. Ekdopayi JN, Iyun JF, Idris SO. Kinetics and mechanism of the electron transfer reaction between sulphite ion and indigo carmine in aqueous acidic medium. *World J Chem.* 2010;5:62-66.

- 38. Imam M, Idris SO, Onu AD. Kinetics and mechanism of the electron transfer reaction of malachite green with sulphite ion in acidic medium. *FUW Trends in Sci Technol J.* 2018;3:778-782.
- 39. Ibrahim I, Idris SO, Abdulkadir I, Onu AD. Kinetics and mechanism of the redox reaction of n, n'-phenylenebis-(salicylideneiminato)iron(III) with oxalic acid in mixed aqueous medium. *Trans Met Chem.* 2019;44:269–273.
- Abdulsalam S, Idris SO, Shallangwa GA, Onu AD. Oxidation of thioglycolic acid by Co(III)salophen in binary mixed DMSO-water and sodium dodecyl sulphate media. Chem Afr. 2024;7:1011-1019.
- 41. Oladunni N, Idris SO, Onu AD, Shallangwa GA. Kinetic and mechanism of oxidation of catechol by oxygenated [Co₂(O₂)(NH₃)₁₀]⁵⁺ complex. *Sci Front*. 2020;2:1-7.
- 42. Chandrawat U, Prakash A, Mehrotra RN. Kinetics and mechanism of the oxidation of the sulphite ion by the Mn(III)-cydta complex ion Canadian J Chemistry. 2011;73:1531-1537.
- 43. Umoru PE, Babatunde OA. Kinetics and Mechanism of the Oxidation of Sulphite Ion by Di-μ-oxo-tetrakis (2, 2' bipyridine)-Dimanganese (III, IV) Perchloratein Aqueous Acidic Medium. *J Chem Soc. Nigeria*. 2019;44:710–717.



The use of Turmeric and Ginger Extracts Mixture as Eco-Friendly Natural Dyes

Zerdeçal ve Zencefil Özleri Karışımının Çevre Dostu Doğal Boyalar Olarak Kullanımı

ABSTRACT

In this study, the dyeing properties of cotton fabric, wool yarn, wool fabric leather and pine wood were investigated by using Turmeric (Curcuma longa L.) and Ginger (Zingiber officinale L.) extracts mixture. For this purpose, these materials were subjected to pre-, meta- and post mordanting processes. Mordanting processes were carried out in the presence of FeSO₄, CuSO₄, AlK(SO₄)₂ and Resadiye clay mordants. The results were evaluated by color analysis of the dyed samples. Rubbing (dry/wet), washing and light fastness values were determined. Color codes, K/S and CIE-Lab values were measured with Konica Minolta CM-3600d Spectrophotometer. Fastness analyses were evaluated using the gray scale acording to ISO 105-C06 standards and CIS. As a result, it was concluded that turmeric and ginger extracts mixture could be a suitable source of dyestuffs for natural dyeing of cotton, wool, leather and wood samples.

Keywords: Ginger, cotton fabric, wool yarn, leather, dyeing, fastness

ÖZ

Bu çalışmada, Zerdeçal (Curcuma longa L.) ve Zencefil (Zingiber officinale L.) ekstraktları karışımı kullanılarak pamuklu kumaş, yün iplik, yün kumaş derisi ve çam ağacının boyama özellikleri araştırılmıştır. Bu amaçla, bu malzemelere ön, meta ve son mordanlama işlemleri uygulanmıştır. Mordanlama işlemleri FeSO₄, CuSO₄, AlK(SO₄)₂ ve Resadiye kil mordanları varlığında gerçekleştirilmiştir. Sonuçlar boyanmış numunelerin renk analizi ile değerlendirilmiştir. Sürtme (kuru/ıslak), yıkama ve ışık haslığı değerleri belirlenmiştir. Renk kodları, K/S ve CIE-Lab değerleri Konica Minolta CM-3600d Spektrofotometresi ile ölçülmüştür. Haslık analizleri ISO 105-C06 standartlarına ve CIS'ye göre gri skala kullanılarak değerlendirilmiştir. Sonuç olarak, zerdeçal ve zencefil ekstraktları karışımının pamuk, yün, deri ve odun numunelerinin doğal boyanması için uygun bir boyarmadde kaynağı olabileceği sonucuna varılmıştır.

Anahtar Kelimeler: Zencefil, pamuklu kumaş, yün iplik, deri, boyama, haslık

INTRODUCTION

Dyeing thread or fabric with vegetable dyes has been done since ancient times and continues today both in our country (Turkey) and in other countries (especially in the Asian continent). Early humans used the roots, stems, leaves and flowers of plants to dye their clothes and ornaments, and sometimes they used stones, soil and some parts of seashells.1

A synthetic dye development process took place from 1771, when the first synthetic dyes were discovered, to 1956, when reactive dyes were discovered, and after that, interest in vegetable dyes gradually decreased.²

K. Ceren TOMBUL APARDIM 1 Adem ÖNAL 1

Mehmet Emin ÇAKMAK 1 Sedanur GÖKÇE¹



¹Department of Chemistry, Faculty of Science, Tokat Gaziosmanpaşa University, Tokat,



Geliş Tarihi/Received 23 02 2025 Kabul Tarihi/Accepted 29.04.2025 Yayın Tarihi/Publication 21.05.2025 Date

Sorumlu Yazar/Corresponding author: Adem Önal,

E-mail: <u>adem.onal@gop.edu.tr</u> Cite this article: Tombul Apardım KC. Önal A, Çakmak ME, Gökçe S. The use of Turmeric and Ginger extracts mixture as eco-friendly natural dyes. J Ata-Chem. 2025;5(1): 20-27.



Content of this journal is licensed under a Creative Commons Attribution-Noncommercial 4.0 International License.

Although synthetic dyes are widely produced and consumed, people in the 21st century still prefer naturally dyed products because natural dyes are healthier than synthetic dyes, and carpets, rugs, ornaments, etc. made from natural dyes. It is a known fact that products gain more value over the years. The only disadvantages of natural dyes compared to synthetic dyes are their low color diversity and low binding power (affinity) to yarn or fabric. Although this is the case for every plant, these problems can often be encountered.³ To solve this problem, people have used mordant substances as binders (fixing the dye) as well as plant parts in dye pots since ancient times. It is known that they use soil and stone containing natural clay, metal oxide or metal salt mixtures.⁴

Different fabric types were examined using Turmeric (*Curcuma longa*.L.). For this purpose, cotton and woolen fabrics were dyed with Curcuma longa extract. Turmeric is not toxic in cell culture and all animal studies. However, it has been reported to have bactericidal effects at very high concentrations that it showed a strong phototoxic effect in micromolar amounts. ^{6,7}

The effect of gamma radiation on dyeing cotton with *Curcuma longa* L. powder was investigated. Dyeing parameters such as temperature, pH and mordant concentration have been optimized. To investigate the effect of radiation, dyeing was done using irradiated and non-irradiated cotton with irradiated and non-irradiated turmeric powder extracts. Color fastness to light, rubbing and washing fastness properties have shown that gamma irradiation improves the dyeing properties moderately.⁸

Ginger (*Zingiber officinale*) is a spice plant that is well known among the public and is used today. In the literature review, a study on dyeing textile fibers with ginger was found. It is noteworthy that more medical studies are being conducted. Ginger, a medicinal aromatic plant, has been used in the treatment of diseases such as rheumatic diseases, respiratory problems, asthma, cough, heart palpitations, migraine and vertigo. 9–11

The aim of this study is to determine the dyeing properties of cellulose and protein type samples using FeSO₄, CuSO₄ and AlK(SO₄)₂ mordants in turmeric and ginger aqueous extract mixture. As a result of the experimental study, the effect of the turmeric/ginger mixture in terms of both dyeing capacity and antimicrobial effect was interpreted according to the results obtained.

METHODS

All mordants (CuSO₄.5 H_2O , FeSO₄.7 H_2O , AlK(SO₄)₂.12 H_2O) were purchased from Merck. The cotton fabric, wool yarn and wool fabric were obtained from Toga

Textile Ltd., Tokat, Turkey. Sheepskin was taken from Maturation Institute, and pine wood samples were obtained from Tokat Organized Industrial Workshop (Tokat, Turkey).

Natural Dye Extraction

30 g of powdered turmeric and powdered ginger were extracted separately with distilled water in a soxhlet apparatus at boiling temperature until colorlessness. Each extract was combined at a ratio of 1/9 for ginger and turmeric after obtaining a total of five liters of colored solution.

Dyeing methods

In this study, the mordants used were prepared as in our previous studies. Pre-mordanting, metamordanting, post-mordanting and without-mordanting methods were performed given below.

Pre-mordanting method

The samples were heated with 100 mL of 0.1 M mordant solution at 90°C (at 40°C for leather) for 20 min. and filtered. After this process, all samples were heated in an erlenmayer with 100 mL of dyestuff solutions at 75°C for 1h. for wool yarn, at 90°C for 1 h. for cotton fabrics, at 90°C for 1 h. for wood, and at 40°C for 2 hours for leather samples. Finally, they were cooled, filtered, rinsed with distilled water and dried.²

Meta-mordanting method

The samples are placed in to the 100 mL of dyestuff solution. Then, solid mordant equivalent to the amount of 0.1 M in 100 mL of the substance was added and heated for 1h. in an erlenmayer with dyestuff at 75°C for 1h. for wool yarn, at 90°C for 1 h. for cotton fabrics, at 90°C for 1 h. for wood, and at 40°C for 2 hours for leather samples. Finally, they were cooled, filtered, rinsed with distilled water and dried. 2

Post-mordanting method

In this method, all samples were heated in an erlenmayer with dyestuff at 75°C for 1h. for wool yarn, at 90°C for 1 h. for cotton fabrics, at 90°C for 1 h. for wood and at 40°C for 2 hours for leather samples. They cooled, filtered, rinsed with distilled water. They were heated with 100 mL of 0.1 M mordant solution at 90°C (for leather at 40°C) for 20 min. Finally, all samples were cooled, filtered, rinsed with distilled water and dried.²

Without-mordanting method

The samples were heated in an erlenmayer with 100 mL of dyestuff solution at 75°C for wool yarn/fabric 1h., at 90°C for 1h. for cotton fabrics, at 40°C for 2 h. for leather, and at 90°C for 1h. for wood samples Finally they were cooled, filtered, rinsed with distilled water and dried.²

RESULTS

Color codes of dyed samples with the dyestuff obtained from turmeric and ginger are given in Table 1, L^* a^*b^* values are given in Table 2, and fastness values are given in Table 3.

The L^* , a^* and b^* values of samples dyed with turmeric/ginger are given in Table 2. Wet, dry, washing and light fastness values of dyed samples are given in Table 3.

When Table 3 is examined, it is seen that good results are obtained with all CuSO₄, FeSO₄, AlK(SO₄)₂ and Reşadiye clay mordants in dry rubbing fastness of cotton fabric, wool fabric, wool yarn and leather samples dyed in turmeric / ginger mixture. Rubbing fastness is 5 for all fabric types.

The highest results in wet rubbing fastness (4-5) are obtained with Reşadiye clay mordant while $CuSO_4$, $FeSO_4$, $AIK(SO_4)_2$ mordants have a lower wet fastness value (2-3) compared to Reşadiye clay.

The highest fastness values (4) in wet rubbing fastness of the samples dyed meta- and with the postmordanting method were obtained with Reşadiye Clay mordant, as in pre-mordanting. On average, the lowest values (2-3) compared to other mordants were observed in fabrics dyed with FeSO₄ mordants. The fastness values of the samples dyed with the mordant-without- mordanting method are lower than the mordant dyeing method, and this result can be interpreted as the chemical bonds formed in the without—mordanting dyeing are lower than the mordant dyeing. Color codes of cotton fabrics dyed with turmeric/ginger mixture are given in Table 1.

When washing fastnesses were examined, a decrease was observed in the order of alum, ferrous sulfate and copper sulfate in washing fastness, while a decrease was observed in the dyeing method in the post-, meta-, and pre-mordanting method. The washing fastness of cotton fabrics is higher than that of woolen fabric and woolen yarn (4-5). In the wash fastness analysis, the best score (5) in

pre-mordanting was given by AIK(SO_4)₂ mordant. In metamordanting, AIK(SO_4)₂ and Reşadiye clay mordant gave the highest value (5), while Reşadiye clay gave the best result (4-5) in the post- mordanting. In without- mordanting dyeing, the best score (5) in washing fastness was obtained in cotton fabrics.

When the light fastness in Table 3 was evaluated, CuSO₄ and FeSO₄ mordant gave the best results (6-7) in premordanting for wool yarn and leather. CuSO₄ mordant gave the best result (cotton fabric 5, wool yarn 7, leather 7) in meta-mordanting, and Reşadiye Clay gave the worst result (cotton fabric 2, wool fabric 1, wool yarn 2).

In the post —mordanting method, CuSO₄ mordant gave the best value in light fastness as in meta-mordanting (cotton fabric 5, wool fabric 4, wool yarn 7, leather 7). The fact that the best light fastness value is obtained in leather samples can be explained by the fact that the leather has a tighter protein structure and consists of more types of amino acid units.

Kocatürk et al.¹⁶ dyed wool fibers with turmeric and natural indigo, they did not determine the fastness and K/S values, they only measured L^* , a^* , b^* values. The values they obtained are in accordance with the values in this study.

Kaynar et al.¹⁷ examined the fastness of colors obtained from turmeric plant with natural and chemical mordants for wool yarns. The color tones they obtained are similar to the color tones we obtained. In this study, dry rubbing fastness values were found to be 2/3 for AlK(SO_4)₂ and 2 for FeSO₄, while these values were 4 for both mordants in our study, which were higher. In the same study, wet rubbing fastness values were found to be 4/5 for AlK(SO_4)₂ and 3 for FeSO₄, while these values were found to be 5 for both mordants in our study.

Scale of cotton fabrics are given in Figure 1, for wool fabrics are in Figure 2, for wool yarns are in Figure 3, for leather samples are in Figure 4 and for wood samples are in Figure 5.

Table 1. Color codes of dyed samples.

Mordant		Heat (°C)	Time (min)	CuSO ₄	FeSO ₄	AIK(SO ₄) ₂	Reşadiye Clay
Pre-	Cotton	90	60	#DACB89	#DBC980	#D8C474	#D7C986
Mordanting	Wool	90	60	#F0DC8D	#EFDA8D	#E4CF83	#EBDA8C
	Wool yarn	90	60	#B69D38	#918233	#A79C40	#A88049
	Leather	40	120	#BF9C45	#A98251	#94645	#917B5B
Meta-	Cotton	90	60	#D4C699	#D1BE84	#D9CF94	#DBD59F
Mordanting	Wool	90	60	#EAD98B	#E6CE9D	#EFDA83	#F5E798
	Wool yarn	90	60	#927447	#9C7438	#D2AA4D	#E8B54D
	Leather	40	120	#625340	#665847	#C59D6B	#AB8851
	Pine wood		2880	#DDB837	#AC8A55	#F5C348	#E8B248
	Cotton	90	60	#DCD6A7	#D8CE95	#D8D395	#D9D7AF
Post- Mordanting	Wool	90	60	#F7EC9E	#F0E18E	#EFE098	#EFE6B5
	Wool yarn	90	60	#E6BB5D	#CDA74F	#CCAB5C	#B3995B
	Leather	40	120	#AE8B5B	#CFAE7F	#BC9363	#C19C6A

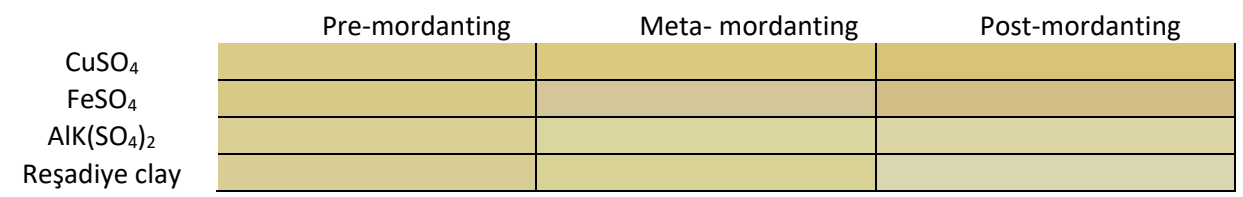


Figure 1. Color scale of cotton fabrics

	Pre-mordanting	Meta- mordanting	Post-mordanting
$CuSO_4$			
FeSO ₄			
$AIK(SO_4)_2$			
Reşadiye clay			

Figure 2. Color scale of wool fabric

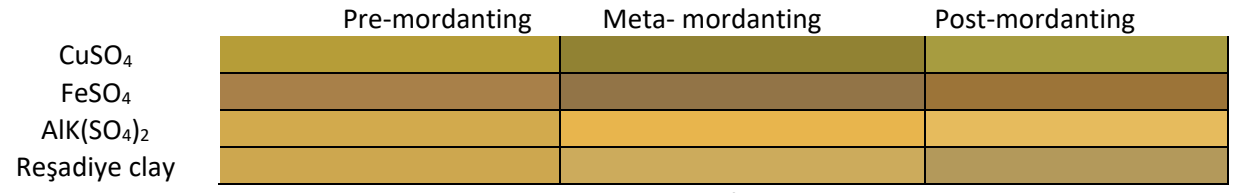


Figure 3. Color Scale of wool yarn

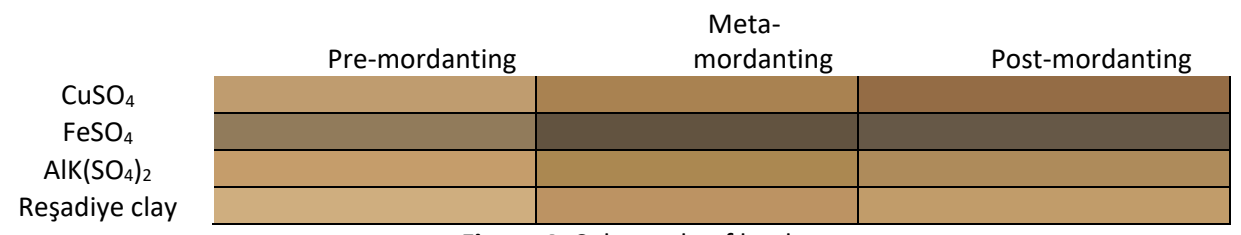


Figure 4. Color scale of leather

Table 2. L* a*b* values of dyed samples.

			Cotton			Wool			Wool yarn			Leather fabric	
Dyeing Method	Mordant	L*	a*	b*	L*	a*	b*	L*	a*	b*	L*	a*	b*
	CuSO ₄	81.6479	-	34.9708	87.7531	-	41.4013	65.3080	-	53.9499	66.5260	7.2769	28.6604
Pre-			4.1641			3.6231			2.0424				
Mordanting	FeSO ₄	80.6534	-	35.0915	86.7749	-	40.5281	56.4342	8.6447	35.5240	53.0165	3.6511	20.9368
			4.3337			4.4042							
	AIK(SO ₄) ₂	82.5815	-	30.4870	87.1028	-	45.3741	71.5580	4.4433	52.3613	67.3996	8.2819	31.9809
			5.2001			4.4167							
	Reşadiye	82.4527	-	29.6656	89.2087	-	42.4587	70.2810	4.1304	49.7137	72.9137	5.8497	28.4178
	clay		5.2071			6.3578							
	CuSO ₄	80.9814	-	38.7291	87.0777	-	40.4056	54.4217	-	43.5251	57.1765	8.8656	32.2563
Meta-			3.7471			2.9016			4.0180				
Mordanting	FeSO ₄	79.9702	-	24.5118	86.5038	-	40.4070	50.7282	6.2509	29.1513	38.3901	2.5694	11.8315
			1.8444			4.5317							
	AIK(SO ₄) ₂	84.4866	-	27.5320	91.2660	-	40.1887	76.6141	8.2100	58.3235	58.7938	6.7996	34.5097
			5.9672			6.3882							
	Reşadiye	83.6890	-	31.4831	88.8579	-	36.8599	71.4885	2.3455	44.6924	63.8464	9.2905	31.4220
	clay		7.5899			4.9581							
	CuSO ₄	79.1343	-	42.1650	83.4222	-	40.3297	63.6006	-	48.4050	48.8846	10.7937	28.1291
Post-			3.2207			2.9411			7.5522				
Mordanting	FeSO ₄	77.3253	-	31.8594	83.7020	1.5685	27.3148	51.6432	9.5072	38.5973	36.1886	3.6141	13.6106
			1.3627										
	AIK(SO ₄) ₂	85.1789	-	24.0254	92.6982	-	39.1505	78.0158	4.7251	52.7204	60.1918	6.9334	30.9254
			5.2509			7.1589							
	Reşadiye	85.3008	-	20.3215	90.8214	-	24.9839	64.3392	1.6904	35.8158	66.5547	7.5357	31.0123
	clay		5.7712			4.1107							

Table 3. Wet, dry, washing and light fastness values of dyed samples.

Dyeing Method				Wet fastnes	S		Dry fastne	ess				Washing fa	stness			Light fast	ness
		CuSO ₄	FeSO ₄	AIK(SO ₄) ₂	Reşadiye clay	CuSO ₄	FeSO ₄	AIK(SO ₄) ₂	Reşadiye clay	CuSO ₄	FeSO ₄	AIK(SO ₄) ₂	Reşadiye clay	CuSO ₄	FeSO ₄	AIK(SO ₄) ₂	Reşadiye clay
	Cotton	5	5	5	5	4	3	4	4	4	5	5	5	3	3	3	2
Pre-	Wool	5	5	5	5	4	4	3	4	3	3	4	3	2	2	1	1
Mordan ting	Wool yarn	5	5	5	5	4	3	4	4	3	3	4	3	6	6	2	3
6	Leather	5	5	5	5	2	3	3	3	4	3	3-4	4	7	7	6	6
	Cotton	5	5	5	5	4	4	4	4	3	3	5	4	5	4	3	2
Meta-	Wool	5	5	5	5	3	3	3	4	2	3	3	4	7	7	3	2
Mordan ting	Wool yarn	5	5	5	5	4	4	4	4	4	4	4	4	4	4	2	1
tii.B	Leather	5	5	5	5	3	2	3	4	3	4	3	4	7	7	6	6
	Cotton	5	5	5	5	4	3	4	4	4	4	4	5	4	4	2	1
Post- Mordan	Wool	5	5	5	5	4	3	4	4	3	3-4	4	4	4	3	2	1
ting	Wool yarn	5	5	5	5	4	3	4	4	3	3	3	4	6	6	2	2
	Leather	5	5	5	5	3	3	4	4	4	4	3	4	7	7	6	6

			Wool fabric	Cotton	Wool yarns	Leather
	Dyeing Method	Mordant	K/S	K/S	K/S	K/S
		CuSO ₄	1.3937	1.22989	9.06506	2.3889
	Pre-	FeSO ₄	1.26854	1.37782	6.52296	4.171175
	mordanting	AIK(SO ₄) ₂	1.51673	0.98052	4.75156	2.5897
		Reşadiye clay	1.20579	0.9680	5.22092	1.56339
	Meta-	CuSO ₄	1.13937	1.49684	12.31667	5.09457
Turmeric/ginger		FeSO ₄	1.27823	0.86968	7.3911	7.41906
extract	mordanting	AIK(SO ₄) ₂	0.90599	0.75671	4.45746	4.95247
		Reşadiye clay	0.91521	0.99645	3.83241	2.17598
		CuSO ₄	1.45602	1.95258	7.94071	7.46135
	Post-	FeSO ₄	0.77595	1.47302	10.70364	9.61682
	mordanting	AIK(SO ₄) ₂	0.76696	0.57565	3.27866	3.85056
		Reşadiye clay	0.43100	0.50019	4.09496	2.63145

Table 4. K/S values of wool and cotton fabrics dyed with turmeric/ginger extracts.

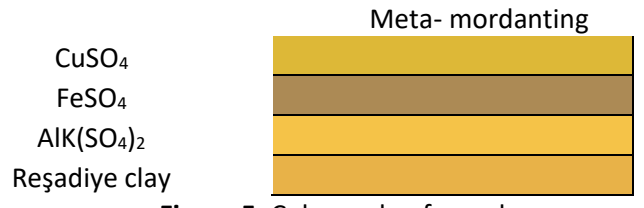


Figure 5. Color scale of wood

The K/S values of cotton fabrics dyed with turmeric/ginger extract are given in Table 4. According to the Table 4, the highest value (K/S=1.95) in the K/S measurements fabrics of cotton dyed turmeric/ginger extract was obtained in the last mordanting method with CuSO₄. The lowest value (K/S = 0.50) was obtained in the last mordanting method with Resadiye claymordant. When we evaluate the Table 4, we can see that the highest value in K/S values of woolen fabrics (K/S= 1.51) was obtained in the pre-mordanting method with AIK(SO₄)₂ mordant. The lowest result (K/S=0.43) was obtained in the post- mordanting method with Resadiye clay mordant. When the data in Table 4 is evaluated, the highest value in the K/S of wool yarns was obtained in the meta- mordanting method with CuSO₄ mordant (K/S=12.31), while the lowest value was obtained with in the last mordant method with AIK(SO₄)₂ mordant (K/S=3.27). According to the Table 4, the highest value (K/S=7.46) in the K/S of the leather dyed with turmeric and ginger was obtained in the post-mordanting method with CuSO₄ mordant, while the lowest value (K/S=1.56) was obtained in the pre-mordanting method with Reşadiye Clay mordant.

In the study conducted by Önal et al.⁵ on the dyeing of different types of fabrics with turmeric extract, the results obtained in wool and cotton fabric dyeing were in the range of (4–5) for CuSO₄ and FeSO₄ in pre-mordanting, together and post- mordanting, and it is noteworthy that they are slightly higher than in our study. The low values we found may be due to the low turmeric concentration in the dye mixture we used. In the same study, the K/S value for cotton fabric was found to be 12.60 for FeSO₄, while it was found to be 1.37 in our study. The highest K/S value for wool yarn was found to be 2.55 for FeSO₄, while the highest K/S value in our study was measured as 1.51. The low results can be explained by the decrease in the turmeric concentration in the dye bath.

DISCUSSION

In the study, the extracts were prepared from dried and ground turmeric and ginger. The samples were dyed with FeSO₄, CuSO₄ and AlK(SO₄)₂ and Reşsdiye clay mordants using pre–, meta–, post–mordanting and without–mordanting methods. When the results obtained in this study were evaluated, it was concluded that the light, washing and friction fastnesses of the dyed samples were at a good level and that turmeric and ginger extracts could be a suitable dye source in natural dyeing of cotton, wool, leather and wood. Additional research is required to increase color efficiency and fastness values. Our working group is making the necessary plans in this regard.

Hakem Değerlendirmesi: Dış bağımsız.

Yazar Katkıları: Veri Toplanması, Analiz: K. Ceren Tombul Apardım; Fikir, Tasarım, Veri Toplanması, Analiz ve Yorum, Literatür Taraması: Adem Önal; Veri Toplanması, Analiz: Mehmet Emin Çakmak; Veri Toplanması, Analiz: Sedanur Gökçe.

Çıkar Çatışması: Yazarlar, çıkar çatışması olmadığını beyan etmiştir. Etik Komite Onayı: Bu çalışma için etik kurul onayı gerekmemektedir. Finansal Destek: Yazarlar, bu çalışma için finansal destek almadığını beyan etmiştir.

Peer-review: Externally peer-reviewed.

Author Contributions: Data Collection, Analysis: K. Ceren Tombul Apardım; Concept, Design, Data Collection, Analysis and Interpretation, Literature Review: Adem Önal; Data Collection, Analysis: Mehmet Emin Çakmak; Data Collection, Analysis: Sedanur Gökçe

Conflict of Interest: The authors have no conflicts of interest to declare. **Ethics Committee Approval:** Ethics committee approval is not required for this study.

Financial Disclosure: The authors declared that this study has received no financial support.

REFERENCES

- Önal A, Gökçe S. Eco-friendly dyeing of leather and wood samples using Parthenocissus quinquefolia L. fruits aqueous extract. J New Res Sci. 2024;13:13-21.
- 2. Gümüştekin S, Önal A, Özbek O, Karaman İ. The use of mint and thyme extracts as eco–friendly natural dyes and the antimicrobial properties of dyed products. *Kuwait J Sci.* 2025;52:100316.
- 3. Önal A, Özbek O, Düzgün P, Nached S. Eco-friendly dyeing of fabric and wool yarn samples with Morus nigra leaf extracts. *J Turk Chem Soc Section A: Chemistr.* 2023;10(3):821-828.
- 4. Özcan Y. Tekstil Elyaf ve Boyama Tekniği. İstanbul Üniversitesi Mühendislik Fakültesi Yayınları. 1984;60:3176.
- Önal A, Tombul KC, Nached S. Investigation of dyeing properties of different fabric species with curcuma longa extracts. Rev Roum Chim. 2020;65:983-988.
- 6. Abdul-Reda Hussein U, Mahmoud ZH, Alaziz KA, et al. Antimicrobial finishing of textiles using nanomaterials. *Braz J Biol*. 2023;84:e264947.
- 7. Fadli M, Bolla JM, Mezrioui NE, Pagès JM, Hassani L. First evidence of antibacterial and synergistic effects of Thymus riatarum essential oil with conventional antibiotics. *Industrial Crops Products*. 2014;61:370-376.

- 8. Bhatti IA, Adeel S, Jamal MA, Safdar M, Abbas M. Influence of gamma radiation on the colour strength and fastness properties of fabric using turmeric (Curcuma longa L.) as natural dye. *Radiat Phys Chemistr.* 2010;79(5):622-625.
- 9. Uysal Bayar F. Doğadan Gelen Mucize: Zencefil (Zingiber Officinale). *Bahçe*. 2020;49:99-110.
- 10. Banerjee S, Mullick HI, Banerjee J, Ghosh A. Zingiber officinale: 'a natural gold'. *Int J Pharmaceutical Bio-Sci.* 2011;2:283-294.
- 11. Mustafa T, Srivastava KC, Jensen KB. Drug development report. 9. Pharmacology of ginger, zingiber-officinale. *J Drug Develop*. 1993;6(1):25-39.
- 12. Çolak H, Gümüştekin S, Önal A, Özbek O, Usta NC. Eco-friendly dyestuffs prepared with Curcuma Longa L. extracts and their antimicrobial activities. *Green Tech Sustainability*. 2025;3(2):100141.
- 13. Önal A, Durdykulyyeva S, Özbek O, Nached S. The use of Hibiscus sabdariffa flower extracts in cotton fabric and wool yarn dyeing. *J Inst Engineers (India): Series E.* 2022;103(2):315-321.
- 14. Önal A, Özbek O, Tombul KC, Nached S. Investigation of the dyeing properties of cotton fabrics and wool yarns using Prunus persica leaf extract. *J Indian Chem Soc.* 2021;98(7):100092.
- 15. Önal A, Özbek O, Vanlıoğlu F, Teker AT, Boyraz D. Investigation of the dyeing properties of the colorant extracted from Juglans regia L. leaves on cellulosic and protein fabrics. *J Turk Chem Soc Section A: Chemistr.* 2021;8(2):453-460.
- 16. Kocatürk YA, Şanlı HS. Doğal indigo ve zerdeçal ile boyanan yün liflerinin subjektif ve objektif değerlendirilmesi. *Ulakbilge Derg.* 2019;7(43):899-911.
- 17. Kaynar H, Tonus E, Uçar Sözmen E. Zerdeçal (curcuma longa) bitkisinden doğa ve kimyasal mordanlarla elde edilen renkler ve tekstil liflerinde kullanımı. İdil. 2019;63:1579-1589.



The Virtual Screening and Molecular Docking Study of New Inhibitors for SARS-COV-2 Papain-Like Protease (PL^{pro})

Alev ARSLANTÜRK BİNGUL ¹

BİNGUL ¹
Necmettin PİRİNCCİOGLU ²



¹Department of Chemistry, Institute of Natural and Applied Sciences, Dicle University, Diyarbakır, Türkiye

²Department of Chemistry, Dicle University, Faculty of Science, Diyarbakır, Türkiye



 Geliş Tarihi/Received
 21.03.2025

 Kabul Tarihi/Accepted
 03.05.2025

 Yayın Tarihi/Publication
 21.05.2025

 Date

Sorumlu Yazar/Corresponding author: *Necmettin PiRiNCCIOĞLU*,

E-mail: pirincn@dicle.edu.tr

Cite this article: Arslantürk Bingül A, Pirinccioğlu N. The virtual screening and molecular docking study of new inhibitors for SARS-COV-2 papain-like protease (PL^{pro}). *J Ata-Chem*. 2025;5(1): 28-37.



Content of this journal is licensed under a Creative Commons Attribution-Noncommercial 4.0 International License.

SARS-COV-2 Papain Benzeri Proteaz (PLpro) İçin Yeni İnhibitörlerin Sanal Tarama ve Moleküler Yerleştirme Çalışması

ABSTRACT

Although global human mobility has normalized after the COVID-19 pandemic, the disease remains a major threat due to the emergence of new variants, keeping it a key target for drug development. Considerable efforts have been put to understand the disease, to create treatment options, and ultimately to eradicate it. It has been shown that these viruses have the largest genome size among all known RNA viruses, with their genome consisting of an RNA strand enclosed in a protein coat. PL^{pro} is an enzymatic protein which is necessary for the replication process of SARS-CoV-2 and during viral infection, it is essential in helping coronaviruses evade the host's innate immune defense. Consequently, targeting PL^{pro} in antiviral drug development could be an effective approach to inhibit viral replication and interfere with signaling pathways in infected cells. This study aims to provide new potential inhibitor candidates for PL^{pro} (PDB: 7LOS) by molecular modelling study. A total of over 2 million molecules from ZINC15 database have been screened against PL^{pro} by structure- based virtual screening, followed by molecular docking. The docking scores of the top five ligands were in the range of -81.57 kcal/mol and -83.19 kcal/mol, which were much better than that of co-crystallized ligand Y97 (-58.25 kcal/mol). The docking results indicated that ligands interact with the key residues (Asp 164, Arg 166, and Glu167) in the active pocket of PL^{pro}. H02 revealed some physicochemical properties as a potential hit according to the ADME results.

Keywords: SARS-CoV-2, PL^{pro} inhibitors, virtual screening, molecular docking, drug design

ÖZ

COVID-19 salgını sonrasında küresel insan hareketliliği normale dönmüş olsa da, hastalık yeni varyantların ortaya çıkması nedeniyle büyük bir tehdit olmaya devam ediyor. Bu sebeple, hastalığı anlamak, tedavi seçenekleri oluşturmak ve nihayetinde ortadan kaldırmak için önemli çabalar sarf edilmektedir. Bu virüslerin, bilinen tüm RNA virüsleri arasında en büyük genom boyutuna sahip olduğu ve genomlarının bir protein kılıfı içinde bulunan bir RNA ipliğinden oluştuğu kanıtlanmıştır. PLpro, SARS-CoV-2'nin replikasyon süreci için gerekli olan enzimatik bir proteinidir ve viral enfeksiyon sırasında koronavirüslerin konağın doğuştan gelen bağışıklık savunmasından kaçmasına yardımcı olmakta görevlidir. Sonuç olarak, antiviral ilaç geliştirmede PLpro'yu hedeflemek, viral replikasyonu inhibe etmek ve enfekte hücrelerdeki sinyal yollarına müdahale etmek için etkili bir yaklaşım olabilir. Bu çalışma, moleküler modelleme çalışmasıyla PLpro (PDB: 7LOS) için yeni potansiyel inhibitör adayları sağlamayı amaçlamaktadır. ZINC15 veritabanından 2 milyondan fazla molekül, yapı tabanlı sanal tarama ve ardından moleküler yerleştirme ile PLpro'ya karşı tarandı. İlk beş ligandın yerleştirme puanları, eş-kristalize ligand Y97'nin (-58,25 kcal/mol) puanlarından çok daha iyi olan -81,57 kcal/mol ve -83,19 kcal/mol aralığındaydı. Yerleştirme sonuçları, ligandların PLpro'nun aktif cebindeki anahtar kalıntılarla (Asp 164, Arg 166 ve Glu167) etkileşime girdiğini gösterdi. ADME sonuçlarına göre H02, potansiyel bir hedef olarak bazı fizikokimyasal özellikler ortaya koydu.

Anahtar Kelimeler: SARS-CoV-2, PL^{pro} inhibitörleri, sanal tarama, moleküler yerleştirme, ilaç tasarımı

INTRODUCTION

Coronavirus disease 2019 (COVID-19) outbreak, known as Wuhan Novel Coronavirus (COVID-19) has raised due to a group of viruses that can affect many animals and cause respiratory infections in humans through transmission.¹⁻⁴ This infection, which spreads rapidly from person to person, has become a major problem for many countries in terms of health and other sociological aspects. 5 Scientists made tremendous efforts to understand the disease, develop treatment methods, and ultimately eliminate the disease entirely. 6,7 An intense work carried out by the biologist has revealed that these viruses have the largest genome size among the known RNA viruses,8 and their genome is composed of an RNA strand surrounded by a protein coat.9 Due to their long RNA genomes, many mutations occur during the copying of genetic material.8 The possible mutations are expected to lead to the emergence of concerning variants. These variants are dangerous for public health and may result in the formation of different strains that could cause future epidemics.

A series of structural proteins, namely nucleocapsid (N), envelope (E), membrane (M), and spike (S), are involved in the virus's mechanism of infecting the host. 10,11 The process begins with the virus binding to the host cell using its surface spike protein (S) to enter the cell through endocytosis. During this process, the angiotensinconverting enzyme 2 (ACE2) receptor on the surface of human cells acts as the target structure for the virus to bind. Once inside the host, the virus releases its singlestranded RNA, which carries its genetic information, allowing this RNA to bind to the host cell's ribosomes. This binding enables the synthesis of several essential enzymatic proteins, including RNA polymerase, the main protease (M^{pro}), and papain-like cysteine protease (PL^{pro}), which are necessary for the replication process for SARS-CoV-2.¹² Consequently, they have been essential targets for antiviral drug development

The critical role of the papain-like protease (PL^{pro}) enzyme in viral replication is due to its function as a cysteine protease. Upon infection, the viral RNA is converted into replicase polyproteins, pp1a and pp1ab. PL^{pro} is involved in the cleavage of non-structural proteins (NSP1-NSP6) from the polyproteins and form replication-transcription complexes. The synthesis of the viral genome and the direction of replication depend on the formation of these complexes.¹³ There are a range of key components of these replication-transcription complexes and NSP3,

including PL^{pro}, plays a role in processing polyproteins and modulating host immune responses.¹⁴

During viral infection, PL^{pro} plays a crucial role in avoiding coronaviruses from the host's innate immune response. PL^{pro} is responsible for removing cellular proteins such as ubiquitin (Ub) and ISG15 (interferoninduced gene, which are involved in initiating the host's innate immune response. Therefore, targeting PL^{pro} in the design of antiviral drugs can be an important strategy to inhibit viral replication and disrupt signaling pathways in infected cells.

The U.S. Food and Drug Administration (FDA) has authorized only a few antiviral drugs for emergency use. Remdesivir (Veklury) and molnupiravir (Lagevrio), although originally developed for other viral infections, have been repurposed for SARS-CoV-2. These drugs work by targeting the viral RNA-dependent RNA polymerase (RdRp) enzyme.¹⁹ Paxlovid, which is used as a combination of two drugs, nirmatrelvir and ritonavir, is another medication for SARS-CoV-2. Nirmatrelvir inhibits the main cysteine protease (Mpro or 3CLpro) of SARS-CoV-2, while ritonavir helps maintain the necessary conditions for nirmatrelvir to reach effective concentrations against SARS-CoV-2.20 Although PL^{pro} is a potential target for SARS-CoV-2 treatment, it has been found that developing effective and applicable inhibitors is challenging. The primary reason for this is the characteristics of the P1 and P2 regions, which do not allow drugs to bind near the cysteine residue in the active site.²¹ Suitable inhibitors for cysteine protease enzymes are identified when the P1 and P2 regions are targeted, and covalent interactions are formed near the cysteine residue in the active site.²² This makes it very difficult to identify new suitable inhibitors for PL^{pro} inhibition and to repurpose existing ones. The drug discovery process was directed to find a new potential target and BL2-groove is now considered as an alternative location of PL^{pro} enzyme.²³⁻²⁵

A range of literature has been reported for the determination of essential roles of PL^{pro}. Dhananjay et al. screened 659 compounds from the NPASS database, and ten compounds were detected as hits and further interaction study was carried out. The compounds demonstrated interactions with the Tyr264, His175, Asp 164, Arg166, Asp302 amino acids residues which are identical with the residues reported in our study. Another study revealed that the screened compounds showed hydrophobic interactions with the Leu162, Gly163, Met208, Pro247, Pro248, Tyr264, Gly266 and Tyr273, hydrophilic interactions with the polar acceptor residues

Arg166 Gln269 and polar donor residues Asp164, Thr301, Glu161. Most of the reported amino acids were also detected in our study.

In this study, it was aimed to determine compounds as candidate inhibitors for PL^{pro} from the public libraries provided by the repositories ZINC 15 by integrating multiple computational approaches namely molecular docking. The best five results of molecules have been detected with the highest docking scores obtained with molecular docking study compared to the co-crystallized ligand and further evaluation have been proceeded. Screening strategy was designed to start with a compound library of over 2 million compounds from the ZINC 15 library. The library provided a large, well-curated set of commercially available compounds in formats (e.g., mol2 with protonation states and 3D conformations) directly compatible with structure-based virtual screening and DOCK 6 workflows. ZINC15 has been extensively utilized in molecular docking studies, previous enabling reproducibility and facilitating comparison with established literature. The compound repository was narrowed due to the large number of molecules in the ZINC databases to focus on the commercially available targets as well as the chemical fulfilling the druglike and ADME properties. Receptor-based screening was performed in compliance with the better ligand-based screening. The compounds were classified according to the ADME and bioavailability properties obtained from screening.

METHODS

Ligand Library Design

The dockable poses of over 2 million compounds extracted from ZINC15²⁴ database were subjected to the virtual screening using Dock 6.7²⁵ to identify molecules with suitable adaptability to PL^{pro}. They were filtrated as only 3D structures aiming to find as many molecules as possible to search for inhibition effect on main protease. Since the ZINC15 includes mol2 file format of molecules compatible with Dock6, the molecules were ready for molecular docking study.

Molecular Docking

As a target protein, x-ray crystal structure of PL^{pro} (PDB:7LOS)²⁶ was obtained from the Protein Data Bank (http://www.rcsb.). PDB entry 7LOS was selected for docking studies due to its high-resolution structure (2.49 Å) of the SARS-CoV-2 papain-like protease (PLpro) in complex

with a non-covalent inhibitor. This structure was chosen because it provides a well-defined binding site, relevant to our study, with a co-crystallized ligand, allowing for accurate comparison of docking results. The docking procedure consists of four main steps. In the first step, both the ligand and the protein are prepared using UCSF Chimera. Initially, the ligand and other non-standard residues are removed from the protein structure. Subsequently, a molecular surface is generated around the protein (excluding hydrogens) using the DMS (Dot Molecular Surface) algorithm, originally developed by Richards²⁸ and later adapted by Connolly.²⁹ Hydrogen atoms are then added to the receptor, and atomic charges are calculated using Chimera. The resulting file is saved in SYBYL mol2 format. The ligand is extracted as a separate file from the crystal structure (PDB ID: 7SOL), hydrogens are added, and its charges are computed in its ionic form using Chimera. The ligand file is also saved in SYBYL mol2 format, without further energy minimization.

In the second step, receptor-based spheres are generated to define the potential binding site. The program sphgen, as implemented in DOCK³⁰, is used to generate spheres based on the molecular surface and surface normal, using minimum and maximum sphere radii of 1.4 Å and 4.0 Å, respectively. Since the binding site is known, a subset of spheres within a defined radius is selected to represent the active site. The program sphere selector, implemented in DOCK 6, is employed to select all spheres located within 10.0 Å root-mean-square deviation (RMSD) of every atom in the crystallographic ligand structure.

The third step involves the generation of the energy grid. This begins with the creation of a grid box surrounding the selected spheres. The coordinates and dimensions of the box are defined as 3.000, 12.000, and 35.000 Å, with a grid size of $30 \times 30 \times 30$ Å. The grid program, as implemented in DOCK 6, is used to generate scoring grids within the defined binding region.

The final step is flexible docking, where the receptor is treated as a rigid body while the ligand is allowed to explore conformational and orientational flexibility.

Absorption, distribution, metabolism, excretion and toxicity (ADMET) prediction

The ADME properties of ligands by SwissADME web service were also defined to identify the physicochemical and drug likeness properties of the ligands. The level of gastrointestinal absorption, blood-brain barrier (BBB) penetration, bioavailability and inhibition efficiency of a

range of hemeproteins namely, CYP1A2, CYP2C19, CYP2C9, CYP2D6, and CYP3A4 enzymes were identified as physicochemical properties of the compounds.

RESULTS

Molecular Docking Studies

The structures of the co-crystallized ligand (Y97) and hits are shown in Figure 1. The validation of the docking process was tested by re-docking of the co-crystallized ligand to the protein by Dock 6.7. The docked pose of the ligand was compared with its x-ray coordinates having a RMSD of 1.383 Å (Figure 2). The docking pose shows a similar conformational pattern with the co-crystallized ligand. The binding mode of Y97 with the protein is demonstrated in Figure 2.

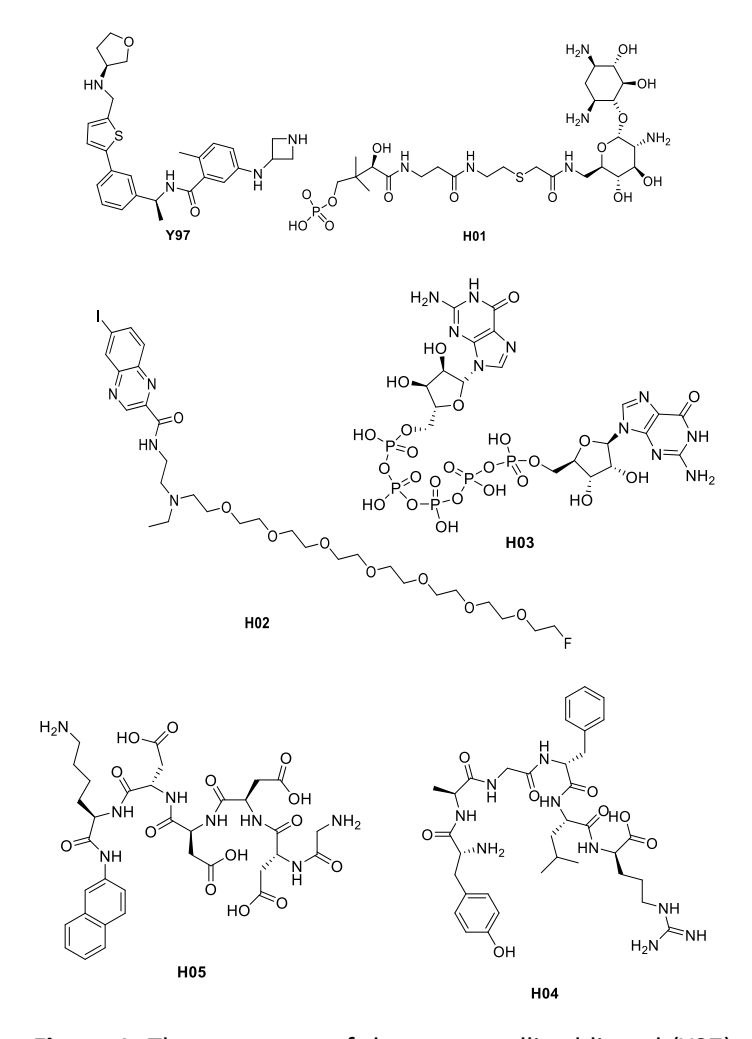


Figure 1. The structures of the co-crystallized ligand (Y97) and hits.

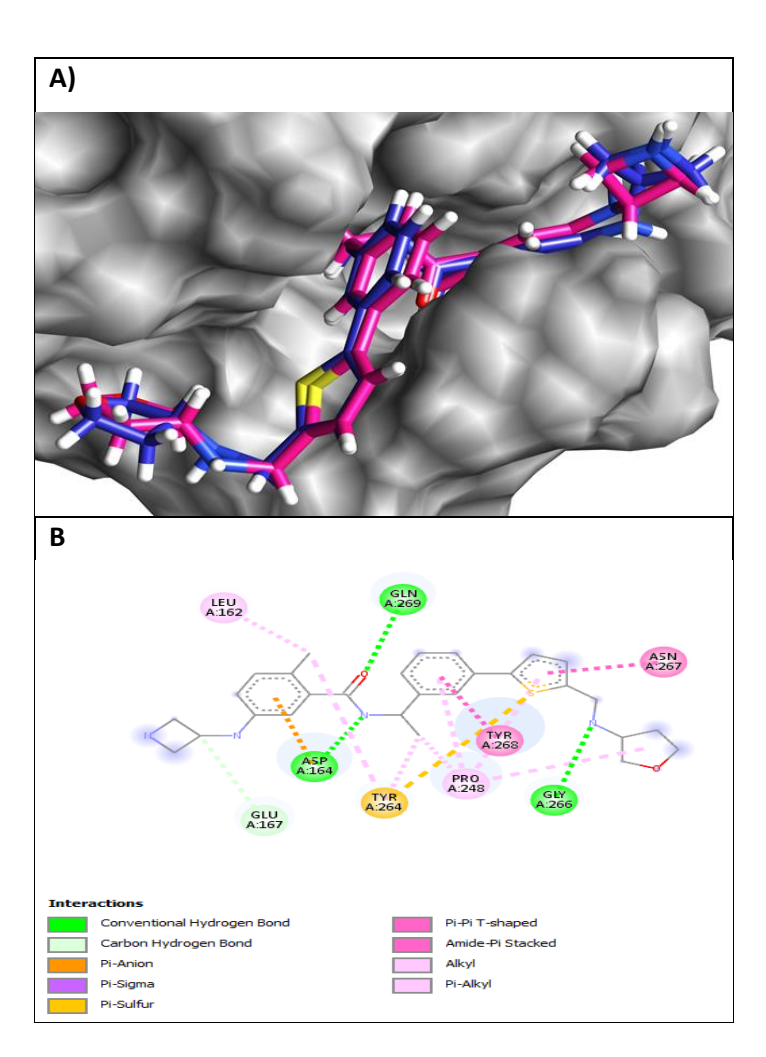


Figure 2. A) The superimposed structure of the cocrystallized ligand (blue) Y97 with the docked pose having a RMSD value of 1.383 Å. B) 2D structure of ligand on catalytic site.

The binding mode of the ligand Y97 involves a range of its interactions with key amino acid residues in the protein. There are diverse interactions, including hydrogen bonds, pi, and hydrophobic interactions. The cyclic amine on the azetidine ring forms a conventional hydrogen bond with Glu167 while the benzene next to the cyclic amine has a pi-sigma and a pi-anion interaction with Asp164. It also interacts with Pro248 via the benzene ring by means of Tshaped pi-alkyl interactions and via the thiophene rings by pi-alkyl interactions. The secondary amine next to the tetrahydrofuran group with interacts with Arg267 through a conventional hydrogen bond and the thiophene ring-with this residue through amide-pi interaction. The amide group also forms a hydrogen bond with Gln 269. Finally, the methyl substitution on the benzene ring interacts with Leu162 via a hydrophobic manner.

Following the validation process, over 2 million compounds were placed into a binding site of PL^{pro}, specifically BL2-groove, molecular docking method. The compounds were sorted according to their docking scores, having the best scores, along with the re-docked cocrystalized ligand were investigated. This study discusses the selected five compounds in terms of having the best docking scores compared to the Y97 ligand and the scores given in Table 1. The scores given in the table are the DOCK 6 scoring function outputs not actual binding free energy. The top five molecules with the highest binding scores were selected for detailed analysis and further in silico evaluations. These compounds, for which the advanced studies (MD simulations and MM-PBSA studies) are ongoing, were chosen to reduce computational costs, limit the number of candidate compounds for experimental validation, and enhance focus by prioritizing the most promising ligands. The information provided in this report is limited to molecular docking results only, as it serves as a preliminary report. According to the results H01 ligand has the best docking score with the value of -83.191 kcal/mol.

Table 1. Scores (DOCK 6 scoring function outputs) of the best five ligands in binding site of PL^{pro} (papain-like protease) obtained from molecular docking studies

_
Dock Score (kcal/mol)
-83.191
-82.422
-82.347
-81.709
-81.574
-58.246

DISCUSSION

Docking studies revealed that hit compounds mainly interact with Gly266, Pro299, Pro248, Tyr264, Arg166, Asp164, Gly163, Gln269, Glu167, Tyr268, Leu162, Lys232, Thr302 and Ser160 residues via hydrogen bonds. The individual binding mode of hits with the protein is demonstrated in Figure 3.

A recent study has highlighted several FDA-approved drugs exhibiting strong binding affinities to the BL2 groove of PLpro. Imatinib, commonly used in leukemia treatment, demonstrated a notable binding affinity with a docking score of -11.95 kcal/mol. Simeprevir used as an antiviral

agent for hepatitis C showed a docking score of -11.20 kcal/mol. Two drugs, Naldemedine and Tucatinib, exhibited identical docking scores of -11.07 kcal/mol and Erdafitinib. prescribed for metastatic urothelial carcinoma, presented a docking score of -10.94 kcal/mol. The binding interactions within the BL2 groove are primarily facilitated by specific residues. Tyr 264 and Tyr 268 residues significantly contribute to ligand binding through hydrophobic interactions. Gln 269 is involved in hydrogen bonding, aiding in ligand stabilization.³¹ Another study revealed that Aspergillipeptide F is one of the best potential PL^{pro} inhibitors. with a pharmacophore-fit score of 75.916 kcal/mol.²⁴ Garland et al. reported some non-covalent PLpro inhibitor through a large scale of virtual screening which the ZINC20 library was used as the source of the compound and experimental study is provided. 32 This study detailed interaction maps provides via crystallography and SPR; confirmed key residues such as Tyr268, Asp164. In our study a detailed in-silico binding mode analysis confirms similar key residues. Importantly, none of the molecule was reported in Garland's study which have been identified as the hit in our study Despite the absence of experimental data, our study provides novel contributions to the computational landscape by offering valuable pharmacokinetic profiles. In addition to that, our manuscript explores novel ligand scaffolds derived from available ZINC15 compounds, some of which show structural divergence from the known GRL-0617 analogs used in Garland et al.32

Most interactions for the H01 occur through conventional hydrogen bonds. The amide group on the long chain forms hydrogen bonds via its NH and carbonyl groups with the amino acid residues Asp 164 and Pro 248, respectively. The thioether linkage and the amino hydrogen on the cyclohexane ring interact with Gln 269. Additionally, the NH group on the cyclohexane scaffold forms an extra hydrogen bond with Leu 162, and Glu 161 forms hydrogen bonds with both the hydroxyl group on the cyclohexane ring and the amine group on the pyran ring. The phosphate group interacts with Arg 166, likely forming a salt bridge through a combination of electrostatic attraction and hydrogen bonding. Furthermore, additional carbon-hydrogen bonds are observed with Asp 164, Leu 162, and Glu 161. Hydrogens on the methylene group near the amide and on the carbon bonded to the cyclohexane hydroxyl group also contribute to these interactions.

The interactions for H02 predominantly occur through conventional hydrogen bonds with various amino acid residues. Lys 232, Tyr 207, Arg 166, and Met 206 form

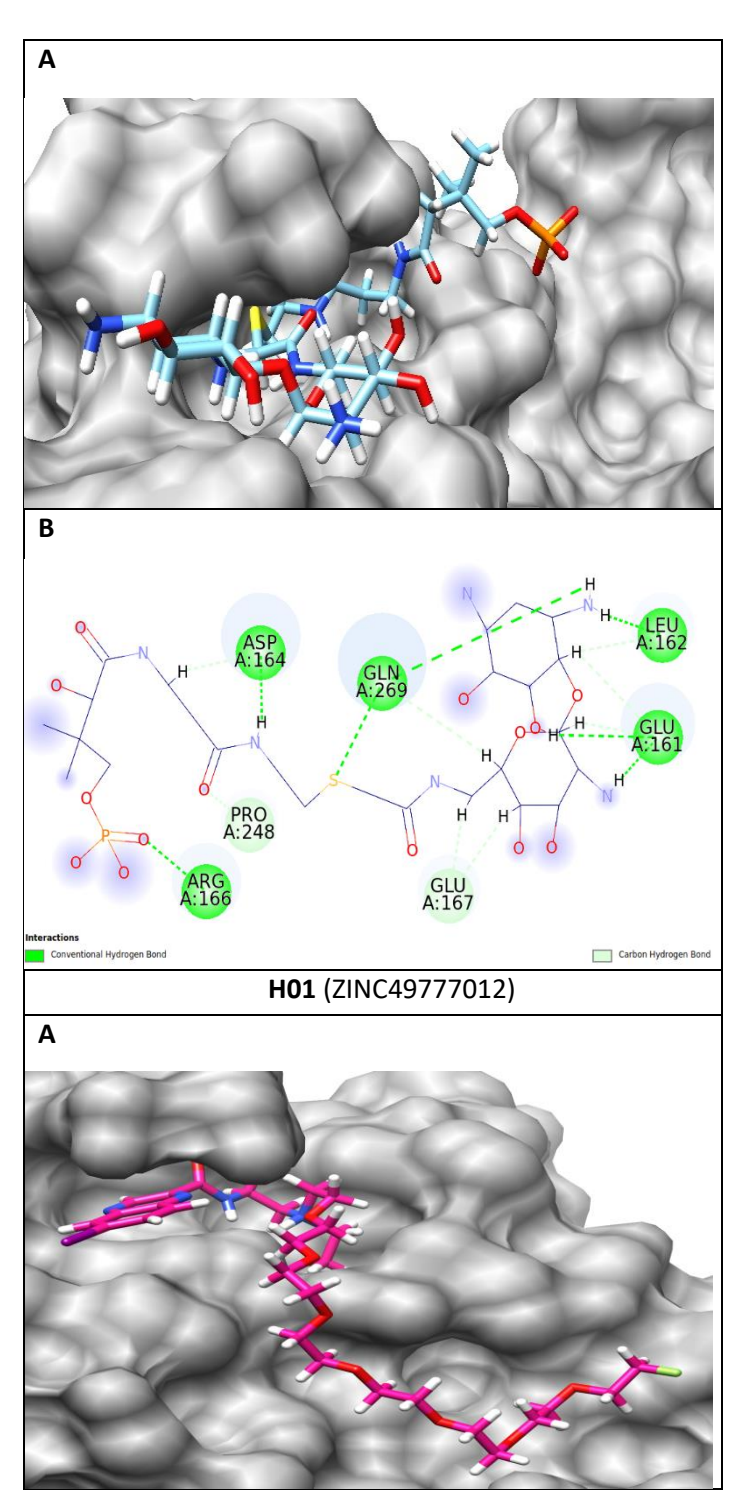
hydrogen bonds with the fluorine and ether functionalities on the polyether chain. Gln 269 establishes a conventional hydrogen bond with the amide carbonyl group near the pyrazine ring. Asp 164 is the residue involved in the most interactions; the tertiary amine nitrogen, the amide nitrogen, and the pyrazine nitrogen all contribute to these interactions. The tertiary amine nitrogen forms a salt bridge with Asp 164, mediated by electrostatic attraction between the positively charged amine group and the negatively charged carboxylate group of Asp 164. Additionally, the pyrazine ring forms a π -anion interaction with Thr 301, and a similar π -anion interaction is observed between the benzene ring attached to the pyrazine and Glu 167.

In the case of H03, the phosphate moiety forms a conventional hydrogen bond exclusively with the Arg 166 residue. It also establishes a salt bridge with Arg 166, involving electrostatic attraction and possibly hydrogen bonding, thereby contributing to the overall stability of the ligand-protein interaction. Carbon-hydrogen bonds involve primarily hydrogen atoms from the tetrahydrofuran ring, which interact with Tyr 268, Glu 167, and Gln 269. Gln 269 engages in a π–sigma interaction with the imidazole ring. The imidazole and pyrimidine rings are responsible for amide π -stacked interactions with Gly 163. Another carbon-hydrogen bond is formed between the pyrimidine NH and Tyr 264. Asp 164 engages in a π-anion interaction with the pyrimidine ring. Pro 299 and Pro 248 contribute π -alkyl interactions with the aromatic imidazole ring. Finally, Glu 266 forms a strong conventional hydrogen bond with the nitrogen atom of the imidazole ring.

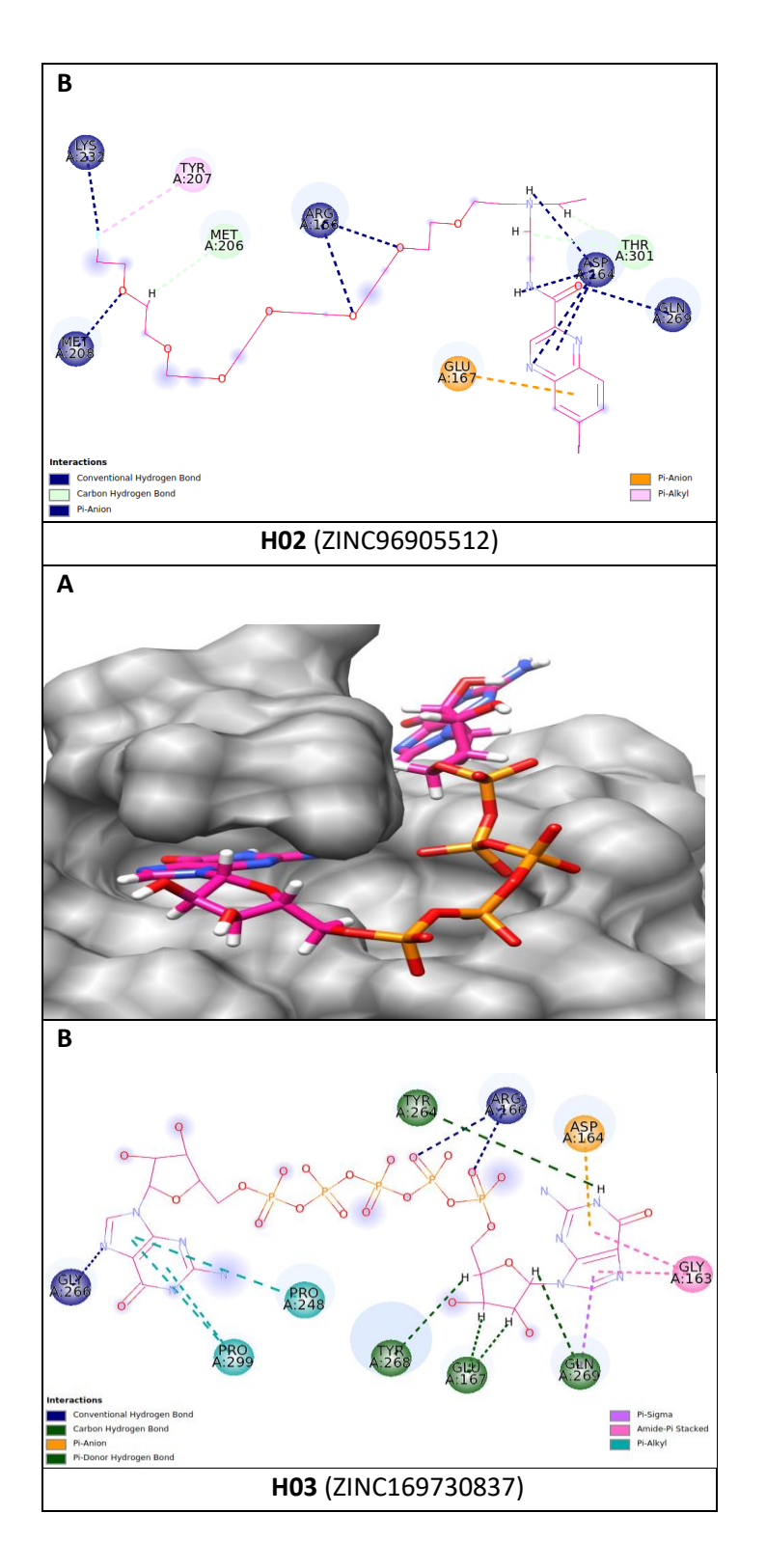
The strongest interactions for H04 occur between the guanidine moiety and the residues Gln 174 and Glu 103. The amide fragment also plays a significant role by forming conventional hydrogen bonds, particularly between the amide carbonyl group and Arg 166. The main salt bridge in this interaction profile is formed between Arg 166 and Glu 103. where electrostatic attraction between the guanidinium group and the carboxylate group contributes to the stability of the ligand-protein complex. Additionally, the amide hydrogen and nearby amino hydrogens form hydrogen bonds with Thr 301 and Tyr 273. Other interactions include a π -alkyl attraction between the isopropyl group and Tyr 171, as well as a carbon-hydrogen bond between the carboxylic acid on the aliphatic linker and Ser 170.

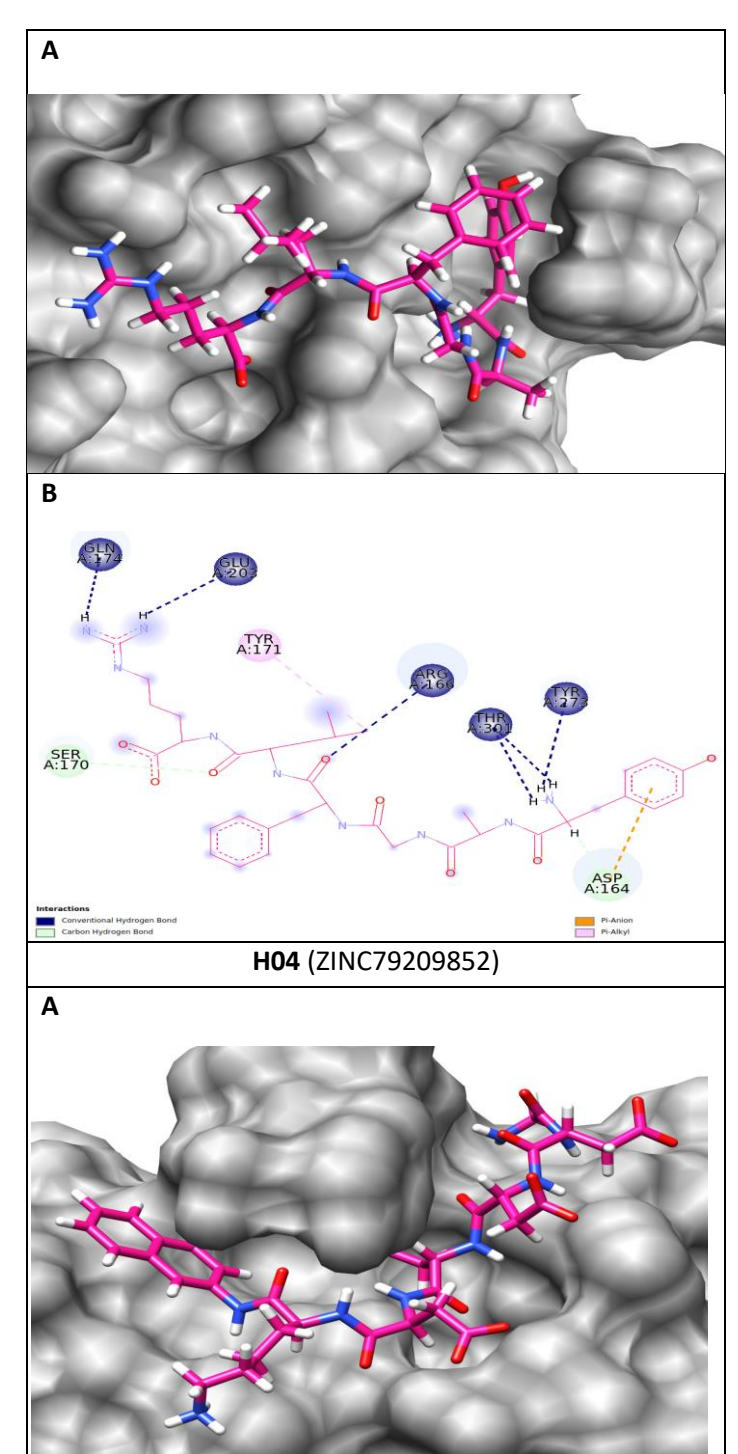
In the case of H05, the amino acid residues primarily interact through conventional hydrogen bonds with the hydrophilic groups of the molecule. The hydrogens of the

amide group form these interactions with Gly 266, Pro 248, Glu 167, and Tyr 268. Additionally, Tyr 268 and Arg 166 establish conventional hydrogen bonds with the amide carbonyl group. Arg 166 also forms a conventional hydrogen bond with the carboxylic acid group, and Tyr 273 participates in this interaction as well. Furthermore, a π -anion interaction occurs between the naphthalene ring and Glu 161, which helps stabilize the overall binding (Figure 3).



J Ata-Chem





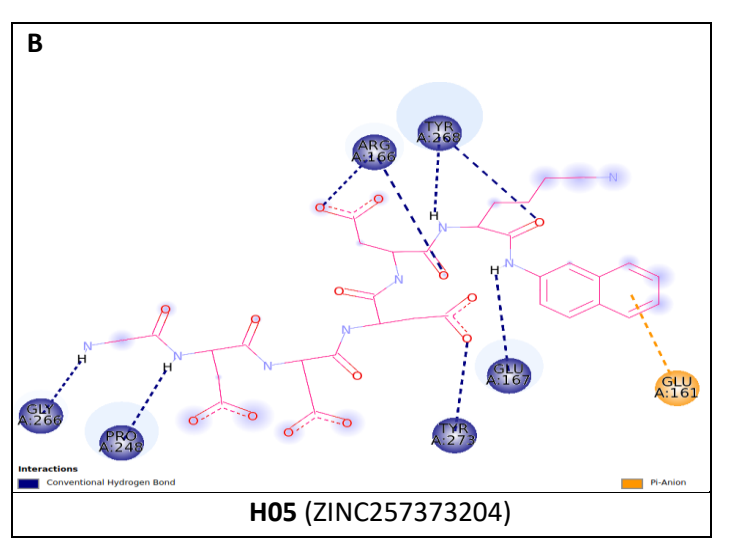


Figure 3. The surface **(A)** and 2D **(B)** structures of the complexes of the ligands with PL^{pro} produced by docking.

ADME results were given Table 2 and 3. According to results, H02 ligand demonstrated high level gastrointestinal absorption property, however none of the ligand showed blood-brain barrier permeation

characteristic (Table 2 and 3). CYP1A2, CYP2C19, CYP2C9, CYP2D6, and CYP3A4 enzymes are different forms of Cytochrome P450 (CYP) protein which are assumed to be crucial for drug metabolism. Analyses revealed that the inhibitory potency of all the ligands was determined at sufficient level toward the CYP1A2, CYP2C19, CYP2C9, CYP2D6, and CYP3A4 enzymes except HIT 02 were found to be effective for the CYP3A4 enzyme inhibition. Bioavailability and molar refractivity results were measured as 0.17 and 167.13, respectively.

Table 2. Physicochemical properties of ligands obtained from SwissADME

Ligand	Molecular mass	H-bond acceptors	H-bond donors	Molar refractivity
H01	720.73	17	13	162.57
H02	724.6	12	1	167.13
H03	948.37	28	13	182.2
H04	725.83	10	11	192.26
H05	788.76	16	12	191.53
				·

Table 3. Predicted ADME properties of the ligands

Ligand	Gl	BBB	Bio	CYP1A2	CYP2C19	CYP2C9	CYP2D6	CYP3A4
	absorption	permeant	Availability					
H01	Low	No	0.17	No	No	No	No	No
H02	High	No	0.17	No	No	No	No	Yes
H03	Low	No	0.11	No	No	No	No	No
H04	Low	No	0.17	No	No	No	No	No
H05	Low	No	0.11	No	No	No	No	No

CONCLUSION

Many compounds were screened against PL^{pro} in a hunt to find potential severe acute respiratory syndrome (SARS-CoV)-2 drugs. A total of five hits were found as potential PL^{pro} inhibitors. It was observed that salt bridges are essential for a favorable binding of ligands to the protein. So, H01 with two salt bridges has the highest docking scores. According to the ADME results H02 were found to be a potential candidate in terms of drug-likeness. Molecular dynamic calculations are further needed to evaluate the binding energies of these ligands and consequently their roles in the conformational changes in the active site of the PL^{pro}.

Hakem Değerlendirmesi: Dış bağımsız.

Yazar Katkıları: Necmettin Pirinccioglu: Konsept; Tasarım; Denetim; Kaynaklar; Analiz ve Yorumlama; Eleştirel İnceleme. Alev Arslantürk Bingul: Veri Toplama ve İşleme; Analiz ve Yorumlama; Literatür Taraması; Makale Yazımı.

Teşekkür: Yazar (AAB), Bilim ve Teknolojide Öncelikli Alanlarda 2211-C Ulusal Doktora Bursu Programı başlıklı burs için TÜBİTAK'a teşekkür etmek ister. Yazarlar ayrıca moleküler yerleştirme işlemi sırasında (TRUBA kaynaklarının) kullanımına izin verdiği için TÜBİTAK ULAKBİM, Yüksek Performans ve Grid Hesaplama Merkezi'ne de minnettardır.

Çıkar Çatışması: Yazarlar, çıkar çatışması olmadığını beyan etmiştir. Etik Komite Onayı: Bu çalışma için etik kurul onayı gerekmemektedir. Finansal Destek: Bu çalışma tüm yazarlar tarafından finanse edilmiştir.

Peer-review: Externally peer-reviewed.

Author Contributions: Necmettin Pirinccioglu: Concept; Design; Supervision; Resources; Analysis and Interpretation; Critical Review. Alev Arslantürk Bingul: Data Collection and Processing; Analysis and Interpretation; Literature Search; Writing Manuscript

Acknowledgements: The author (AAB) would like to thank TUBİTAK for the scholarship entitled as 2211-C National PhD Scholarship Program in

the Priority Fields in Science and Technology. Authors are also grateful to TUBİTAK ULAKBIM, High Performance and Grid Computing Center, for allowing the use of (TRUBA resources) during the molecular docking process.

Conflict of Interest: The authors have no conflicts of interest to declare. **Ethics Committee Approval:** Ethics committee approval is not required for this study.

Financial Disclosure: The authors declared that this study has received no financial support.

REFERENCES

- 1. Cui J, Li F, Shi ZL. Origin and evolution of pathogenic coronaviruses. *Nat Rev Microbiol*. 2019;17:181–192.
- 2. Malik YA. Properties of coronavirus and SARS-CoV-2. Malays. *J Pathol.* 2020;42:3–11.
- 3. Palayew A, Norgaard O, Safreed-Harmon K, Andersen TH, Rasmussen LN, Lazarus JV. Pandemic publishing poses a new COVID-19 challenge. *Nat Hum Behav.* 2020;4:666–669.
- 4. Tu YF, Chien CS, Yarmishyn AA, et al. A review of SARS-CoV-2 and the ongoing clinical trials. *Int J Mol Sci.* 2020;21:2657.
- 5. Li Q, Guan X, Wu P, et al. Early transmission dynamics in wuhan, China, of novel coronavirus—infected pneumonia. *N Engl J Med*. 2020;382:1199–1207.
- 6. Al-Aly Z, Xie Y, Bowe B. High-dimensional characterization of post-acute sequelae of COVID-19. *Nature*. 2021;594:259–264.
- 7. Zhou P, Yang XL, Wang XG, et al. A pneumonia outbreak associated with a new coronavirus of probable bat origin. *Nature*. 2020;579:270–273.
- 8. Satarker S, Nampoothiri M. Structural proteins in severe acute respiratory syndrome coronavirus-2. *Arch Med Res.* 2020;51:482–491.
- 9. Schoeman D, Fielding BC. Coronavirus envelope protein: current knowledge. *J Virol*. 2019;16:1–22.
- Artika IM, Dewantari AK, Wiyatno A. Molecular biology of coronaviruses: current knowledge. *Heliyon*. 2020;6:4743-54.
- 11. Benvenuto D, Giovanetti M, Ciccozzi A, Spoto S, Angeletti S, Ciccozzi M. The 2019-new coronavirus epidemic: evidence for virus evolution. *J Med Virol.* 2020;92:455–459.
- 12. Gao H, Dai R, Su R. Computer-aided drug design for the pain-like protease (PL^{pro}) inhibitors against SARS-CoV-2. *Biomed Pharmacother.* 2023;159:114247.
- 13. Kim H, Hauner D, Laureanti JA, Agustin K, Raugei S, Kumar N. Mechanistic investigation of SARS-CoV-2 main protease

- to accelerate design of covalent inhibitors. *Sci Rep.* 2022;12:21037.
- 14. Malone B, Urakova N, Snijder E, Campbell EA. Structure and function of the coronavirus replication-transcription complex. *Nature Reviews Microbiol.* 2022;20(3):181–194.
- Mielech AM, Kilianski A, Baez-Santos, YM, et al. MERS-CoV papain-like protease has delSGylating and deubiquitinating activities, *Virology*. 2014;450(451):64– 70
- 16. Lindner HA, Lytvyn V, Ql H, et al., Selectivity in ISG15 and ubiquitin recognition by the SARS coronavirus papain-like protease. *Arch Biochem Biophys.* 2007;466(1):8–14.
- 17. Barretto N, Jukneliene D, Ratia K, et al. The papain-like protease of severe acute respiratory syndrome coronavirus has deubiquitinating activity. *J Virol*. 2005;79(24):15189–15198.
- 18. Zhou P, Yang XL, Wang XG, et al., A pneumonia outbreak associated with a new coronavirus of probable bat origin. *Nature*. 2020;579(7798):270–273.
- Jayk Bernal A, Gomes da Silva MM, Musungaie DB, et al. Molnupiravir for Oral Treatment of Covid-19 in Nonhospitalized Patients. N Engl J Med. 2022;386:509–520.
- Eng H, Dantonio AL, Kadar EP, et al. Disposition of Nirmatrelvir, an Orally Bioavailable Inhibitor of SARS-CoV-2 3C-Like Protease, across Animals and Humans. *Drug Metab Dispos*. 2022;50:576–590.
- 21. Xia Z, Sacco M, Hu Y, et al. Rational Design of Hybrid SARSCoV-2 Main Protease Inhibitors Guided by the Superimposed Cocrystal Structures with the Peptidomimetic Inhibitors GC-376, Telaprevir, and Boceprevir. ACS Pharmacol Transl Sci. 2021;4:1408–1421.
- 22. Ma C, Sacco MD, Hurst B, et al. Boceprevir, GC-376, and calpain inhibitors II, XII inhibit SARS-CoV-2 viral replication by targeting the viral main protease. *Cell Res.* 2020;30: 678–692.
- 23. Ferreira GM, Pillaiyar T, Hirata MH, Poso A, Kronenberger T. Inhibitors induced conformational changes in SARS-COV-2 papain-like protease. *Sci Rep.* 2022;12:11585.
- 24. Thangavel N, Albratty M. Pharmacophore model-aided virtual screening combined with comparative molecular docking and molecular dynamics for identification of marine natural products as SARS-CoV-2 papain-like protease inhibitors. *Arabian J Chem.* 2022;15:1-12
- 25. Jadhav P, Huang B, Osipiuk J, et al. Structure-based design of SARS-CoV-2 papain-like protease inhibitors. *Eur J Med Chem.* 2024;264:116011.

- Dhananjay J, Selvaraj A, Vyshnavi T, et al. Virtual high throughput screening: Potential inhibitors for SARS-CoV-2 PL^{PRO} and 3CL^{PRO} proteases. *Eur J Pharma*. 2021;901:174082,
- Deepesh KP, Harish KM, Elizabeth S. Exploring the binding dynamics of covalent inhibitors within active site of PL^{pro} in SARS-CoV-2. Comp Bio Chem. 2024;12:108132.
- 28. Richards FM. Areas, volumes, packing, and protein structure. *Ann Rev Biophys Bioeng*. 1977;6:151–176.
- 29. Connolly ML. Solvent-accessible surfaces of proteins and nucleic acids. Dissertation. University of California, Berkeley; 1981.
- 30. Kuntz ID, Blaney JM, Oatley SJ, Langridge R, Ferrin TE. A geometric approach to macromolecule-ligand interactions. *J Mol Biol.* 1982;161(2):269–288.
- 31. Ashouri M, Firouzi R. Virtual Screening and Binding Mode Analysis of Selected FDA Approved Drugs Against PL^{pro} Target: An Effort to Identify Therapeutics to Combat COVID-19. *Med Discoveries*. 2023;2(9):1070.
- 32. Garland O, Ton AT, Moradi S, et al. Large-scale virtual screening for the discovery of SARS-CoV-2 papain-like protease (PLpro) non-covalent inhibitors. *J Chem Inform Model*. 2023;63(7):2158–2169.